AD 273 328

STEVENS INSTITUTE OF TECHNOLOGY

CASTLE POINT STATION
HOBOKEN, NEW JERSEY

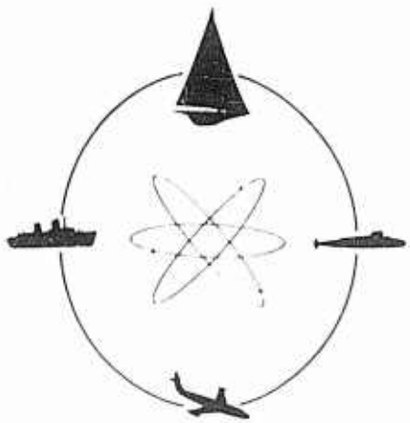

DAVIDSON LABORATORY

HYDROFOIL FLUTTER PHENOMENON AND AIRFOIL FLUTTER THEORY

by Charles J. Henry

VOLUME I
DENSITY RATIO

R-856 SEPTEMBER 1961

HYDROFOIL FLUTTER PHENOMENON AND AIRFOIL FLUTTER THEORY

by Charles J. Henry

VOLUME I
DENSITY RATIO

DL Project LG2247
Report R-856
September 1961

PREPARED UNDER
OFFICE OF NAVAL RESEARCH
CONTRACT Nonr 263(35)

DAVIDSON LABORATORY
Stevens Institute of Technology
Castle Point Station
Hoboken, New Jersey

FOREWORD

The theoretical background for the study of hydroelastic problems, recently introduced to the designers of naval craft, has been taken mostly from the analogous field of aeroelasticity. Two problems in hydrofoil design that have received some attention are flutter (oscillatory divergent motion) and divergence (exponentially divergent motion). The boundary between stable and unstable motion in each case is the critical flutter-speed or critical divergence-speed. This volume discusses only critical flutter-speed.

This research was carried out under the Bureau of Ships Fundamental Hydromechanics Research Program, S-R009-01-01, administered by the David Taylor Model Basin, Office of Naval Research Contract Nonr 263(35).

The author wishes to express his gratitude to Professor Holt Ashley of the Department of Aeronautics and Astronautics of the Massachusetts Institute of Technology for his helpful comments, Professor Paul Ritger of the Department of Mathematics of Stevens Institute of Technology for his contribution to this report, and Mr. Raihan Ali, Research Engineer at Davidson Laboratory, for the reduction of data used in this analysis.

TABLE OF CONTENTS

		Page
Foreword		
Abstract		
I.	Introduction	1
II.	Test Setup	3
	A. Model and Supports	3
	B. Instrumentation	5
	C. Weights	6
III.	Theoretical Analysis	11
	A. General	11
	B. Equations of Motion	11
	C. Critical Density Ratio	22
IV.	Discussion	23
	A. General	23
	B. Experimental Procedure	23
	C. Experimental Results	24
	D. Theoretical Results	25
V.	Theory Compared with Experiments	27
VI.	Conclusions	29
VII.	Recommendations	31

LIST OF TABLES

Table

I. Properties of Model Tenite II, Formula 233, Flow MS

II. Parameters and Flutter Conditions

III. Typical Results from Superposition Calculations

LIST OF ILLUSTRATIONS

Figure

1. Previous Experimental Results
2. Test Apparatus
3. Apparatus, Starboard Side
4. Apparatus, Port Side
5. Balance, Starboard Side
6. Balance, Port Side
7. Flexure Balance
8. Representative Hydrofoil Orientation for Theoretical Analysis
9. Schematic Diagram of System used for Dynamic Analysis
10. Reduced Flutter-Speed versus Density Ratio
11. Overall Damping Ratio versus Reduced Speed (Stability Analysis, Series 0, $\mu = 0.758$)
12. Overall Damping Ratio versus Reduced Speed (Stability Analysis, Series 1, $\mu = 0.883$)
13. Overall Damping Ratio versus Reduced Speed (Stability Analysis, Series 2, $\mu = 1.008$)
14. Overall Damping Ratio versus Reduced Speed (Stability Analysis, Series 4, $\mu = 1.285$)
15. Overall Damping Ratio versus Reduced Speed (Stability Analysis, Series 7, $\mu = 2.08$)
16. Overall Damping Ratio versus Reduced Speed (Stability Analysis, Series 9, $\mu = 3.03$)
17. Overall Damping Ratio versus Reduced Speed (Stability Analysis, Series 11, $\mu = 4.07$)

Figure

18. Frequency Ratio versus Reduced Speed (Stability Analysis, Series 0, μ = 0.758)

19. Frequency Ratio versus Reduced Speed (Stability Analysis, Series 1, μ = 0.883)

20. Frequency Ratio versus Reduced Speed (Stabiltiy Analysis, Series 2, μ = 1.008)

21. Frequency Ratio versus Reduced Speed (Stability Analysis, Series 4, μ = 1.285)

22. Frequency Ratio versus Reduced Speed (Stability Analysis, Series 7, μ = 2.08)

23. Frequency Ratio versus Reduced Speed (Stability Analysis, Series 9, μ = 3.03)

24. Frequency Ratio versus Reduced Speed (Stability Analysis, Series 11, μ = 4.07)

25. Critical Density-Ratio

NOMENCLATURE

Symbol	Definition
a	dimensionless distance in half-chord lengths from midchord to rotational axis, positive if the rotational axis is aft
b	half-chord length
c	chord length, $c = 2b$
$C(k)$	Theodorsen function
d, e, f, ℓ	quantities defined in Eq. 26
h	translation displacement of model from equilibrium
h_o	initial amplitude of simple harmonic translatory motion
H, J	quantities defined in Eq. 32
$H'(s)$	dimensionless downwash velocity at 3/4 chord
i	integral index, $i = 1, 2, 3...$
I_c	mass polar moment of inertia of rotating parts about its center of gravity, per unit span
I_α	mass polar moment of inertia of rotating parts about the rotational axis, per unit span
I_{α_n}	value of I_α for the nth mass condition
ΔI_{α_i}	the ith change in I_{α_n}, $\Delta I_{\alpha_i} = I_{\alpha_{i+1}} - I_{\alpha_i}$
J	imaginary unit, $j = \sqrt{-1}$
k	reduced frequency, $k = \omega b/U$
K_h	support stiffness in translation per unit span

Symbol	Definition
K_α	support stiffness in rotation per unit span
ℓ_i	length of ith cylindrical weight in second group
$\mathfrak{L}$	the Lagrangian
$\mathfrak{L}^{-1}$	inverse Laplace transformation operator
L,M	unsteady hydrodynamic lift and moment, per unit span
L_h, L_α, M_h, M_α	dimensionless unsteady hydrodynamic coefficients, complex functions of k, tabulated in references 9 and 10
L_{hr}', L_{hi}', $L_{\alpha r}'$ $L_{\alpha i}'$, M_{hr}', M_{hi}' $M_{\alpha r}'$, $M_{\alpha i}'$	dimensionless unsteady hydrodynamic coefficients, real functions of k and a, defined in Eq. 26
m	total oscillating mass per unit span, $m = m_\alpha + m_h$
m_a	mass required in weight group 1 to attain desired mass
m_h	mass of translating parts per unit span
m_n	total mass of nth mass condition
m_α	mass of rotating and translating parts, per unit span
m_b	value of m for apparatus with no weights added
Δm_i	the ith change in m_n, $\Delta m_i = m_{i+1} - m_i$
n	index giving mass condition, numbered successively starting with the lowest value, n = 1, 2, 3...
p	complex Laplace transform variable
P(p)	fifth order complex polynomial in p
Q_h	generalized force

Symbol	Definition
Q_α	generalized moment
$Q(p)$	sixth order complex polynomial in p
r_α	dimensionless radius of gyration about rotational axis, $r_\alpha^2 = I_\alpha/mb^2$
R	radius of cylindrical weights in group 2
$R(p)$	fifth order complex polynomial in p
s	dimensionless time variable, $s = Ut/b$
S_{α_n}	first moment of mass of rotating parts in the nth mass condition, about the rotational axis, per unit span
t	time
u,v	real and imaginary parts of the Laplace transform variable, $p = u + j\,v$
u_1, u_2	real roots of Eq. 46 given in Table III
U	free stream velocity
$W(s)$	dimensionless circulatory response function giving unsteady lift and moment for an arbitrary motion, defined in Eq. 36
$\bar{x}_a$	distance from desired center of gravity location to the center of gravity of m_a
$\bar{x}_b$	distance from desired center of gravity location to the center of gravity of m_b
x_α	dimensionless distance in half-chords from the rotational axis to the center of gravity of m_α, positive if the c.g. is aft
α	rotation displacement of model from equilibrium position, positive for leading edge up
α_o	initial amplitude of simple harmonic rotary motion
β	coupling mass coefficient, $\beta = m_\alpha/m$

Symbols	Definition
δ	indicates virtual displacement
λ	complex eigenvalue of equations of motion, $\lambda = -\sigma + j\omega$
μ	density ratio, $\mu = m/(\pi\rho b^2)$
μ_n	value of μ for the nth mass combination
$\Delta\mu_i$	the ith change in μ_n, $\Delta\mu_i = \mu_{i+1} - \mu_i$
μ_{cr}	critical density ratio
ρ	mass density of water
ρ_2	mass density of weights in second group
σ	real part of $-\lambda$, determines decay rate of oscillatory motion
ϕ	phase angle between h and α, positive when h is leading
$\phi(s)$	Wagner function
ψ	dimensionless λ, $\psi = \lambda b/U$
ω	imaginary part of λ, circular frequency of oscillatory motion
ω_h	uncoupled natural frequency in translation, $\omega_h^2 = K_h/m$
ω_α	uncoupled natural frequency in rotation, $\omega_\alpha^2 = K_\alpha/I_\alpha$
Ω_h	dimensionless natural frequency in translation, $\Omega_h = \omega_h b/U$
Ω_α	dimensionless natural frequency in rotation, $\Omega_\alpha = \omega_\alpha b/U$
$\dot{}$	indicates differentiation with respect to t
$'$	indicates differentiation with respect to s
$-$	indicates Laplace transformation

ABSTRACT

The theoretical procedures commonly used by aeroelasticians were applied to predict the flutter speed of a rigid hydrofoil that had two degrees of freedom. The results, compared with corresponding experimental measurements, indicated a discrepancy between theoretical and experimental flutter speeds at low density ratios; the predicted asymptotic behavior of flutter speeds occurred, but at a lower density-ratio. In addition, the accuracy of the circulation terms is more doubtful than that of the added mass and linear terms in the theory.

I. INTRODUCTION

Destructively large stresses or undesirable levels of vibration have been induced in airfoils operating near the critical flutter-speed. Theoretical and experimental investigations have shown that for certain elementary elastic configurations, flutter of foils in water is unlikely (references 1, 2, 3, and 4). Figure 1 shows the range of density ratios applicable to these simple hydrofoil-configurations. The magnitude of the dynamic pressure encountered by submerged control surfaces--rudders, stabilizing fins, hydrofoils, bow planes, etc.--is greater than that encountered by airfoils, except for those used on recent, high-speed aircraft. Therefore, one is led to the following question: why have hydrodynamic control surfaces not experienced flutter?

In particular, bending-torsion flutter of cantilever-supported hydrofoils has been investigated (reference 3). In this investigation, a critical density-ratio was predicted below which flutter was not possible. Isolated experiments using simple supports, confirmed these results. In these experiments, no flutter was obtained and none predicted. However, the low, overall damping associated with the unsteady hydrodynamic forces on the rudders of a destroyer, which recently experienced severe and sustained hull vibrations, has provided the impetus for further investigations of hydrodynamic flutter (reference 5). Cursory investigations of this vibration indicate that more realistic support conditions, and other conditions, may reduce the lowest value of density ratio at which hydrofoils will flutter. Therefore, the reliability of theoretical predictions of flutter speed at low values of density ratio must be determined.

In previous hydroelastic work, it was assumed that aerodynamic theories would apply directly to the hydrodynamic problem. Assuming this to be true, these theories should correctly predict the flutter speed of a hydrofoil. This investigation was conducted to experimentally verify the accuracy of aeronautical theories when used to predict flutter speed (throughout the range of parametric values of interest in hydrofoil design).

Some previous work along these lines has been performed. The NACA investigated flutter of light, cantilever-supported wings in an airstream made heavy by the use of Freon and air mixtures (reference 4). The experimental points in Figure 1 are representative of the results obtained by NACA. The range of density ratio in this investigation did not extend into that for a cantilever-supported hydrofoil. However, the range of density ratio in which flutter was obtained experimentally extends, by a small amount below the critical density-ratio, into the range in which flutter is theoretically impossible. It is this discrepancy which was investigated.

In view of the inconclusiveness of previous experimental and theoretical results, a single set of experiments was conducted over a range of density ratio extending from region 1 through regions 2 and 3 and well into region 4 (Figure 1).

In these experiments, speed and density ratio were varied; all other parameters were constant. Another series of experiments is being conducted at several additional values of center-of-gravity location and radius of gyration to investigate further the discrepancy between theory and experiment.

II. TEST SETUP

A. MODEL AND SUPPORTS

The experimental setup was designed so that flutter would be obtained under controlled conditions that closely duplicated the theoretical assumptions; the setup did not typify any hydrofoil application (Figures 2 through 6). The experiments were performed in the High-Speed Facility.

The model had a chord length (c) of 6 inches and a span of 12 inches. The profile was a thin symmetrical shape, (NACA 0012). The offsets for the model were obtained from reference 6. The material used for the model was a plastic whose properties are summarized in Table I.

1. End Plates

End plates were used to provide two-dimensional flow and were attached to the carriage by struts and aluminum box-beams. The chord plane of the model was arranged vertically and the end plates were above and below the model, each with a maximum clearance of 0.006c. The end plates were 11.29c long by 6.71c wide. The rotational axis of the model was located in the middle and 4.31c aft of the leading edge of the end plates. The end plates were made of 1/8-inch aluminum plates stiffened in both the transverse and longitudinal direction. The transverse stiffening members were covered with aluminum sheets, which provided fairing to reduce drag.

2. Sting Support

The model was supported by a vertical sting that passed through the upper end-plate and the water surface to a flexure balance that was entirely above water. The sting was a stainless-steel tube (1-inch OD, 0.87-inch ID, BWG No. 16)

protected from the stream velocity in the region between the upper end-plate and the water surface by a faired shield.

To reduce the effect of the hole in the upper end-plate, a small, circular plate made of 1/16-inch stainless steel was attached to the lower end of the sting. The radius of this auxiliary end-plate overlapped the hole in the upper end-plate when the sting was displaced to either side. The auxiliary end-plate was below the main end-plate and had a maximum clearance of 0.006c.

3. Balance

The sting was attached to the fixed support through a flexure balance (Figures 5, 6, and 7). Two modes of motion for the model in the horizontal plane were permitted by this balance; rotation about a vertical, spanwise axis and horizontal translation normal to the direction of motion. Mechanical stops limited these motions to $\pm 3/4$-inch of translation and ± 2 degrees of rotation. The axis of the sting was in line with the quarter-chord axis of the model and was located at the apex of a pair of V-frames (Figure 7). These frames, located in parallel horizontal planes one above the other, provided a linear elastic restoring moment in the desired rotational degree of freedom and were effectively rigid in all other degrees of freedom. These frames were I-beams with lightening holes in the webs and were necked down at both ends as shown in Figure 7. Most of the flexibility of these beams was concentrated in the necked-down sections (flexures); the dimensions of the flexures were chosen to give the desired rotational stiffness. The base of the V-frames was connected to the fixed support through four parallel bars, which allowed the whole unit to translate in the desired direction. In a manner similar to the members of the V-frames, the ends of the parallel bars were necked down to provide the desired translation flexibility (Figure 7). The translation bars were aluminum channels and the rotation beams were machined aluminum stock.

A spring-loaded, locking mechanism was installed that held the model in the desired initial position until it was released by a solenoid controlled by a switch at the operators station.

The flexure balance was anchored to the carriage by a supporting structure. To provide greater rigidity against rotation of the apparatus in the vertical transverse plane, an outrigger was attached to an auxiliary wheel that ran along the side of the tank.

The apparatus satisfied all requirements for the support of the model. The rotation spring stiffness came within 8% of the desired value and the translation spring stiffness came within 3%. These errors arose mainly from the estimate of the effect of fillets at both ends of the flexures. A flexure length equal to the actual flexure length, including both fillets, minus one fillet radius, gave values for predicted stiffnesses within 2% of the measured values. The rigidity of support against undesired motions was found to be well within reasonable limits. The frequency of vertical translatory oscillations of the model in air was found to be three times greater than the highest frequency encountered during the tests in water. All other observed frequencies of extraneous motions were five or more times the highest test frequency.

B. INSTRUMENTATION

The motions of the model were measured by recording the unbalance of strain-gage bridges. Strain gages were mounted on the flexure balance and the signal outputs from the strain-gage bridges were recorded. To measure the speed of the apparatus, an electronic counter was used to determine the time required for the apparatus to pass between two locations a known distance apart. In addition, a tachometer generator, attached to the carriage, was activated by a wheel running on the carriage rail to measure the instantaneous speed of the

apparatus. The average speeds obtained by these two methods were in agreement and no appreciable speed fluctuations during the runs were observed.

In general, slide rule accuracy was maintained throughout the experimental analysis. Scatter in the data is a result of actual extraneous effects in the experiments and is not caused by inaccuracies in the instrumentation.

The parametric values obtained in the experiments are shown in Table II. In view of the large amount of weight added externally and rigidly to the foil, the results of the experiments described here should not be viewed as representative of any hydrofoil application. In practice, density ratios greater than 1.0 are seldom encountered, if ever.

The experimental flutter speeds and frequencies are given in Table II and the results are plotted in Figures 10 through 24. The corresponding theoretical results are presented along with these results.

C. WEIGHTS

Two sets of weights were connected rigidly to the sting to obtain the selected center-of-gravity (c.g.) location ($x_\alpha b$), radius-of-gyration ($r_\alpha b$), uncoupled natural frequency ratio (ω_h/ω_α), and to vary the density ratio (μ_n) while maintaining all other parameters as constants (Table II).

The uncoupled natural frequency in each mode of vibration can be defined as follows:

$$\omega_h^2 = K_h/m \quad \text{and} \quad \omega_\alpha^2 = K_\alpha/I_\alpha \tag{1}$$

where K_h = support stiffness in translation per unit span

K_α = support stiffness in rotation per unit span

m = total oscillating mass per unit span

I_α = mass polar moment of inertia of rotating parts about the rotational axis, per unit span.

The dimensionless radius of gyration can be defined as follows:

$$r_\alpha^2 = I_\alpha / mb^2 \tag{2}$$

where b is the half-chord length of the model. When equations 1 and 2 are combined, the uncoupled natural frequency ratio is

$$(\omega_h/\omega_\alpha)^2 = (K_h/K_\alpha)\ (r_\alpha b)^2 \tag{3}$$

Thus, the stiffness ratio (K_h/K_α) is determined by the values of ω_h/ω_α, r_α, and b.

Let the subscript b denote the characteristics of the apparatus without weights and the subscript a denote the characteristics of the apparatus with the first set of weights. Let the subscript n = 0, 1, 2, ... denote the desired values of the properties numbered successively, starting with the smallest mass condition. Therefore, the necessary additional mass (m_a) can be determined as follows:

$$m_a = m_o - m_b = \mu_o \pi \rho b^2 - m_b \tag{4}$$

where μ_o = density ratio of initial mass-condition = $m_o/\pi\rho b^2$

ρ = mass density of water.

To find the required location of the c.g. of m_a, the moment of mass about the selected c.g. location is set equal to zero as follows:

$$\bar{x}_a m_a + \bar{x}_b m_b = o \tag{5}$$

where $\bar{x}$ is the distance from the selected c.g. location to the c.g. of the mass indicated.

Equations 4 and 5 were used to determine the amount of mass necessary to obtain the initial mass-condition and the location of the c.g. of this mass. The distribution of m_a was selected to provide the required mass polar moment of inertia $(I_{\alpha o})$. Therefore, two weights, each with mass $m_a/2$, were symmetrically placed on either side of the c.g. location $(\bar{x}_a)$. The distance between the masses was adjusted until

$$I_{\alpha_o} = (r_\alpha b)^2 m_o. \tag{6}$$

In this manner, the desired values of x_α, r_α, ω_h/ω_α, in addition to the initial value of density ratio (μ_o), were obtained. The second set of weights were designed to provide the selected values of μ_n while maintaining a, x_α, r_α, and ω_h/ω_α constant.

The position of the rotational axis (ab) and the stiffness ratio (K_h/K_α) were fixed; these properties remained unchanged throughout the experiments. The desired x_α was obtained with the first set of weights. To keep the c.g. location constant, the c.g. of the second set of weights was put at the selected c.g. location and thus did not change x_α. Equation 3 shows that ω_h/ω_α will remain constant as m increases when r_α is constant. Therefore, the ratio I_α/m was kept constant as the weights were added.

At each mass condition (n), the moment of inertia (I_{α_n}) and the mass (m_n) may be divided into the sum of the respective values for the lowest mass condition plus the increment due to each weight added (i = 1, 2, ..., n - 1).

$$\left.\begin{aligned} I_{\alpha_n} &= I_{\alpha_o} + \sum_{i=1}^{n} \Delta I_{\alpha_i} \\ m_n &= m_o + \sum_{i=1}^{n} \Delta m_i \end{aligned}\right\} \quad n = 1, 2... \tag{7}$$

By substituting these quantities into the definition of the radius of gyration, equation 2 yields

$$I_{\alpha_o} + \sum_{i=1}^{n} \Delta I_{\alpha_i} = (r_\alpha b)^2 \left[m_o + \sum_{i=1}^{n} \Delta m_i\right], \tag{8}$$

and subtracting equation 6 from equation 8 leaves

$$\sum_{i=1}^{n} \Delta I_{\alpha_i} = (r_\alpha b)^2 \sum_{i=1}^{n} \Delta m_i, \tag{9}$$

which must hold for all n. Therefore,

$$\Delta I_{\alpha_i} = (r_\alpha b)^2 \Delta m_i. \tag{10}$$

A cylindrical shape was chosen for the weights with radius R_1 and length ℓ_1 and with axis at the desired c.g. location. The mass polar moment of inertia of the ith weight per unit span about the rotational axis is given by

$$\Delta I_{\alpha_1} = \frac{\Delta m_1}{2} R_1^2 + \Delta m_1 \, (x_\alpha b)^2. \tag{11}$$

Equation 11 combined with equation 10 shows that:

$$R_1 = b \left[2(r_\alpha^2 - x_\alpha^2) \right]^{1/2}. \tag{12}$$

But the right-hand side is independent of i. Therefore, the subscript may be dropped from R. The length of the ith weight is governed by the required change in mass, as follows.

$$\ell_1 = \frac{\Delta m_1}{\pi \rho_2 R^2} \tag{13}$$

where ρ_2 is the mass density of the second set of weights.

III. THEORETICAL ANALYSIS

A. GENERAL

In hydrofoil applications, an adequate definition of flutter properties can be obtained from a study of the stability of very small motions. Small motions should be stable; otherwise, they lead to fatigue conditions if not to larger destructive motions. In practice, the large motions usually are stable if the small motions are stable. Therefore, time dependence can be assumed to be proportional to $e^{\lambda t}$, where λ is a complex number; all other motions can be built up by superposition. (The procedure for superposing the lift response for more complicated motions is given in Appendix A.)

During flutter, the critical flutter-speed is associated with a frequency of sustained vibratory motion. The determination of the critical flutter-speed becomes a simpler problem when simple harmonic motion is assumed; it is easier to describe mathematically the hydrodynamic loads for simple harmonic motion than it is to describe these loads for more general motions. Therefore, to simplify the problem, the speed and frequency required for sustained simple harmonic motion should be determined, rather than the response of the foil system as a function of speed. In this investigation, all time dependent terms for simple harmonic motion were assumed proportional to $e^{j\omega t}$ (ω real), rather than $e^{\lambda t}$. Figure 8 shows the coordinates and nomenclature used in this investigation.

B. EQUATIONS OF MOTION

The equations of motion for the experimental model were derived from Lagrange's equations. A lumped-parameter

system, with negligible damping due to friction or structural deformations, was assumed representative of the model. Figure 9 shows the dynamic system and the following definitions were used:

m_h = mass of translating parts per unit span;

m_α = mass of rotating parts per unit span;

I_c = mass polar moment of inertia of rotating parts about its center of gravity per unit span.

The Lagrangian for the translation and rotation displacements [$h(t)$ and $\alpha(t)$] is

$$\mathfrak{L} = \frac{1}{2}m_h\dot{h}^2 + \frac{1}{2}m_\alpha(\dot{h} + x_\alpha b\dot{\alpha})^2 + \frac{1}{2}I_c\dot{\alpha}^2 - \frac{1}{2}K_h h^2 - \frac{1}{2}K_\alpha\alpha^2. \quad (14)$$

By substituting $\mathfrak{L}$ into Lagrange's equation, the equations of motion for the system are

$$m\ddot{h} + m_\alpha x_\alpha b\ddot{\alpha} + K_h h = Q_h, \quad (15)$$

and

$$I_\alpha\ddot{\alpha} + m_\alpha x_\alpha b\ddot{h} + K_\alpha\alpha = Q_\alpha, \quad (16)$$

where the dots indicate differentiation with respect to t and the following definitions have been used:

$m = m_h + m_\alpha$ = total oscillating mass per unit span,

$I_\alpha = I_c + (x_\alpha b)^2 m_\alpha$ = mass polar moment of inertia of rotating parts about the rotational axis per unit span.

Q_h and Q_α, are the generalized force and moment, respectively, acting on the system. By considering the work done by external forces during a virtual displacement (δh and $\delta\alpha$), Q_h and Q_α became the hydrodynamic lift and moment per unit span at the rotational axis.

The equations of motion can be put in non-dimensional form by dividing equation 15 by $\pi\rho bU^2$ and equation 16 by $\pi\rho b^2U^2$ and by using the following non-dimensional parameters:

$\mu = m/\pi\rho b^2$ = density ratio,

$\beta = m_\alpha/m$ = coupling mass ratio,

$\Omega_h^2 = K_h b^2/mU^2$ = dimensionless uncoupled natural frequency in translation,

$\Omega_\alpha^2 = K_\alpha b^2/I_\alpha U^2$ = dimensionless uncoupled natural frequency in rotation,

$r_\alpha^2 = I_\alpha/mb^2$ = dimensionless radius of gyration about rotational axis,

$s = Ut/b$ = dimensionless time variable, and

$h(s)$, $\alpha(s)$ = dimensionless translation and rotation displacements

so that

$$h(s) = \frac{1}{b}h(t) \quad \text{and} \quad \alpha(s) = \alpha(t). \tag{17}$$

By introducing these quantities and by nondimensionalizing, the equations of motion become

$$\mu\, h'' + \beta\mu\, x_\alpha \alpha'' + \mu\Omega_h^2 h = L/\pi\rho\, bU^2 \tag{18}$$

and

$$\mu r_\alpha^2 \alpha'' + \beta\mu x_\alpha h'' + \mu\, r_\alpha^2 \Omega_\alpha^2 \alpha = M/\pi\rho\, b^2U^2 \tag{19}$$

where the primes indicate differentiation with respect to s.

1. Flutter Analysis

The description of the mode shape associated with the flutter of a hydrofoil connected to a hull involves the superposition of the normal vibration modes of the complete structure. When this precise mode shape is used in flutter analyses it results in a lengthy computation because there are an infinite number of normal vibration modes.

Aeroelastic computations have shown that flutter speed and frequency can be predicted accurately by the Rayleigh-Ritz procedure. With this procedure, the mode shape is approximated by the superposition of a finite number of pre-assigned or assumed modes. The choice of modes is governed by the structure involved and by the results desired. Reference 7 discusses the choices available and the criterion

for their use. An accurate and simple procedure is to use two or three primitive mode shapes that are compatible with the boundary conditions. The assumed modes method of flutter analysis has been compared with a more exact treatment (reference 3). The two methods reasonably agreed in the range of parameters used in hydrofoil design.

In this investigation, the assumed modes method exactly described the flutter mode of vibration; the two degrees of freedom of translation and rotation in the plane of flow are the only appreciable displacements of the model. A linear combination of these displacements exactly described the flutter mode-shape. Thus, no approximation was used in the application of the assumed modes method.

In this case, it was more convenient to divide the equation of motion by $\pi\rho b^3\omega^2$ and $\pi\rho b^4\omega^2$ rather than use equations 18 and 19. Introducting the assumption of simple harmonic motion in the form

$$h = h_o b e^{j\omega t} \quad \text{and} \quad \alpha = \alpha_o e^{j\omega t} \tag{20}$$

and using the quantities μ, x_α, and r_α, the equations of motion were

$$\mu\left[1 - \left(\frac{\omega_h}{\omega_\alpha}\right)^2\left(\frac{\omega_\alpha}{\omega}\right)^2\right] h_o e^{j\omega t} + \mu\beta x_\alpha \alpha_o e^{j\omega t} = L/\pi\rho b^3\omega^2 \tag{21}$$

and

$$\mu\beta x_\alpha h_o e^{j\omega t} + \mu r_\alpha^2\left[1 - \left(\frac{\omega_\alpha}{\omega}\right)^2\right] \alpha_o e^{j\omega t} = M/\pi\rho b^4\omega^2 \tag{22}$$

At this point, an explicit representation of the hydrodynamic loads was introduced. The Theodorsen results cited in reference 8 were used in this analysis. In the design of the experimental apparatus, every effort was made to model the assumptions involved in the theory--that is, large endplates were provided with small clearances to preserve two-dimensional flow; the foil supports were designed so that

the desired, rigid-body motions were achieved at every point along the span of the foil; no free surface, cavitation, ventilation or sidewall effects were permitted. In addition, the foil motions were assumed to be sinusoidal; however, the recorded motions were checked only visually.

The representation of the hydrodynamic loads was taken from reference 9, where the expressions for the hydrodynamic lift and moment are given as

$$L = \pi\rho b^3\omega^2 \left\{ L_h h_o + \left[L_\alpha - \left(\frac{1}{2} + a\right) L_h \right] \alpha_o \right\} e^{j\omega t} \qquad (23)$$

and

$$M = \pi\rho b^4\omega^2 \left\{ \left[M_h - \left(\frac{1}{2} + a\right) L_h \right] h_o + \left[M_\alpha - \left(L_\alpha + M_h\right)\left(\frac{1}{2} + a\right) + L_h \left(\frac{1}{2} + a\right)^2 \right] \alpha_o \right\} e^{j\omega t}. \qquad (24)$$

In these relations, ab is the distance from midchord to the rotational axis and is positive if the rotational axis is aft. The coefficients L_h, L_α, M_h, and M_α are complex functions of the reduced frequency (k), which is

$$k = \frac{\omega b}{U} \qquad (25)$$

A tabulation of these coefficients may be found in references 9 and 10.

These results were introduced into the equations of motion with the following notation:

$$L_{hr}' = L_{hr}$$
$$L_{hj}' = L_{hj}$$
$$L_{\alpha r}' = L_{\alpha r} - \left(\frac{1}{2} + a\right) L_{hr}$$
$$L_{\alpha j}' = L_{\alpha j} - \left(\frac{1}{2} + a\right) L_{hj}$$
$$M_{hr}' = M_{hr} - \left(\frac{1}{2} + a\right) L_{hr}$$
$$M_{hj}' = M_{hj} - \left(\frac{1}{2} + a\right) L_{hj}$$

$$M_{\alpha r}' = M_{\alpha r} - (\tfrac{1}{2} + a)(L_{\alpha r} + M_{hr}) + (\tfrac{1}{2} + a)^2 L_{hr}$$

$$M_{\alpha j}' = M_{\alpha j} - (\tfrac{1}{2} + a)(L_{\alpha j} + M_{hj}) + (\tfrac{1}{2} + a)^2 L_{hj}$$

$$d = L_{hr}'M_{\alpha j}' + L_{hj}'M_{\alpha r}' - L_{\alpha r}'M_{hj}' - M_{\alpha j}'M_{hr}'$$

$$e = L_{hr}'M_{\alpha r}' - L_{hj}'M_{\alpha j}' - L_{\alpha r}'M_{hr}' + L_{\alpha j}'M_{hj}'$$

$$f = L_{\alpha j}' + M_{hj}'$$

$$\ell = L_{\alpha r}' + M_{hr}' \tag{26}$$

The subscripts r and j denote the real and imaginary parts of the corresponding complex numbers. Equations 23, 24, and 26 were introduced into equations 21 and 22 and $e^{j\omega t}$ which is common to all terms was cancelled, yielding:

$$\left\{\mu\left[1 - \left(\frac{\omega_h}{\omega_\alpha}\right)^2\left(\frac{\omega_\alpha}{\omega}\right)^2\right] + L_{hr}' + jL_{hj}'\right\} h_o + \left\{\mu\beta x_\alpha + L_{\alpha r}' + jL_{\alpha j}'\right\} \alpha_o = 0 \tag{27}$$

and

$$\left\{\mu\beta x_\alpha + M_{hr}' + jM_{hj}'\right\} h_o + \left\{\mu r_\alpha^2\left[1 - \left(\frac{\omega_\alpha}{\omega}\right)^2\right] + M_{\alpha r}' + jM_{\alpha j}'\right\} \alpha_o = 0. \tag{28}$$

These are the equations of motion that the unknowns h_o, α_o, U, and ω must satisfy.

Equations 27 and 28 are complex, homogeneous, simultaneous linear algebraic equations in the unknown amplitudes h_o and α_o. A nontrivial solution for these unknowns exists, if and only if the determinant of their coefficients vanishes. In this case, the determinant is complex and results in two simultaneous equations by setting the real and imaginary parts of the expanded determinant equal to zero separately. The solution is thus reduced to finding the eigenvalues for U and ω which satisfy two algebraic equations.

However, U appears in equations 27 and 28 only implicitly in the argument (k) of the hydrodynamic coefficients.

Because these coefficients are most easily handled in tabular form rather than functional, the argument usually is considered as an independent parametric variable. The unknown frequency and one other parameter are then considered the dependent unknowns and solutions to the expanded determinant are found at chosen values of k. The second unknown is usually chosen so that one of the equations resulting from the expansion of the determinant is linear in both dependent unknowns. One method of solution of the flutter determinant is the density variation method. Alternate means of solution are described in reference 7.

2. Density Variation Method

The density variation method was particularly appropriate here, because the density ratio was varied while other parameters were kept constant. Thus, the density ratio and the square of the unknown frequency ratio were taken as the dependent unknowns in solving the flutter determinant, which is:

$$\begin{vmatrix} \mu\left[1-\left(\frac{\omega_h}{\omega_\alpha}\right)^2\left(\frac{\omega_\alpha}{\omega}\right)^2\right]+L_{hr}'+jL_{hj}' & \mu\beta x_\alpha+L_{\alpha r}'+jL_{\alpha j}' \\ \mu\beta x_\alpha+M_{hr}'+jM_{hj}' & \mu r_\alpha^2\left[1-\left(\frac{\omega_\alpha}{\omega}\right)^2\right]+M_{\alpha r}'+jM_{\alpha j}' \end{vmatrix}=0 \tag{29}$$

By expanding and setting the imaginary part of the resulting equation equal to zero, the following linear relation exists between the chosen dependent unknowns:

$$\frac{1}{\mu}=\frac{1}{d}\left[\left(\frac{\omega_h}{\omega_\alpha}\right)^2 M_{\alpha j}'+r_\alpha^2 L_{hj}'\right]\left(\frac{\omega_\alpha}{\omega}\right)^2-\frac{1}{d}\left[M_{\alpha j}'+r_\alpha^2 L_{hj}-\beta x_\alpha f\right]; \tag{30}$$

d and f are defined in equation 26. By setting the real part of the expanded determinant equal to zero, and eliminating $1/\mu$ by introducing equation 30,

$$\left(\frac{\omega_\alpha}{\omega}\right)^4 \left\{ r_\alpha^2 \left(\frac{\omega_h}{\omega_\alpha}\right)^2 - H\left[\left(\frac{\omega_h}{\omega_\alpha}\right)^2 M_{\alpha r}' + r_\alpha^2 L_{hr}'\right] + eH^2 \right\}$$

$$- \left(\frac{\omega_\alpha}{\omega}\right)^2 \left\{ r_\alpha^2 \left[1 + \left(\frac{\omega_h}{\omega_\alpha}\right)^2\right] + J\left[\left(\frac{\omega_h}{\omega_\alpha}\right)^2 M_{\alpha r}' + r_\alpha^2 L_{hr}'\right] \right.$$

$$\left. - H\left[M_{\alpha r}' + r_\alpha^2 L_{hr}' - \beta x_\alpha \ell\right] - 2HJe \right\}$$

$$+ r_\alpha^2 - (\beta x_\alpha)^2 + J\left[M_{\alpha r}' + r_\alpha^2 L_{hr}' - \beta x_\alpha \ell\right] + eJ^2 = 0, \qquad (31)$$

which contains only one unknown $(\omega_\alpha/\omega)^2$, in quadratic form. The expressions for H and J are defined by equation 30 so that

$$\frac{1}{\mu} = H\left(\frac{\omega_\alpha}{\omega}\right)^2 + J \qquad (32)$$

At chosen values of k, equation 31 is solved for values of $(\omega_\alpha/\omega)^2$, which are substituted into equation 30 to determine μ. Finally, the corresponding values of the reduced speed are found from the following relationship:

$$\frac{U}{b\omega_\alpha} = \frac{1/k}{\left(\frac{\omega_\alpha}{\omega}\right)} \qquad (33)$$

This method of flutter analysis, including appropriate elastic and dynamic assumptions, is believed to be most useful in hydrofoil design procedures. The results of this analysis applied to the experimental conditions are shown in Figure 10.

The Theodorsen representation of the hydrodynamic forces limited this analysis strictly to simple harmonic motions in two degrees of freedom. If other motions are involved, which are either not simple harmonic or other degrees of freedom, this analysis is not applicable. Subject to these restrictions, the curve of reduced flutter speed versus density ratio obtained by the density variation method defines the condition--that is, speed (U) and frequency (ω)--that must prevail at flutter for a particular hydrofoil section. At speeds above critical flutter-speed, the motion of the

foil will be oscillatory divergent and at lower speeds the motion will be convergent. The curve plotted in Figure 10 is the boundary between unstable motion at higher speeds and stable motion at lower speeds.

3. Stability Analysis

In the stability analysis, the time dependence of the motions again was assumed to be $e^{\lambda t}$. Therefore, from the equations of motion, a characteristic equation was derived, which was a polynomial in λ. The characteristic values (the roots of the polynomial) were found and a quantitative measure of stability was obtained from considering the magnitude and sign of the real parts of all roots. In this sense, the assumed modes method of flutter analysis is not a stability analysis because of the simplifying assumption of sinusoidal motion.

In this analysis, the equations of motion in non-dimensional form were used:

$$\mu h'' + \mu\beta x_\alpha \alpha'' + \mu\Omega_h^2 h - L/\pi\rho b U^2 = 0 \qquad (18)$$

and

$$\mu r_\alpha^2 \alpha'' + \mu\beta x_\alpha h'' + \mu r_\alpha^2 \Omega_\alpha^2 \alpha - M/\pi\rho b^2 U^2 = 0. \qquad (19)$$

The hydrodynamic terms are introduced by the Duhamel superposition integral and the Wagner function $\phi(s)$, which gives the time dependence of the circulatory lift response to a unit step change in angle of attack. The development of these expressions and the following results are described in Appendix A of this report and in references 7 and 10. The Theodorsen representation of the lift and moment is not applicable to this analysis (Appendix B).

The hydrodynamic force and moment are

$$-L/\pi\rho b U^2 = h'' + \alpha' - a\alpha'' + 2W(s) \qquad (34)$$

and

$$-M/\pi\rho b^2 U^2 = ah'' + \left(\frac{1}{2} + a\right)\alpha' + \left(\frac{1}{8} + a^2\right)\alpha'' - 2\left(\frac{1}{2} + a\right)W(s) \qquad (35)$$

In these equations, the quantity $W(s)$ is defined as

$$W(s) = H'(0)\phi(s) + \int_0^s \phi(s - \sigma)H''(\sigma)\,d\sigma, \tag{36}$$

where

$$H'(s) = h' + \alpha + (\tfrac{1}{2} - a)\alpha' \tag{37}$$

and where $H'(0)$ is the value of $H'(s)$ at $s = 0$. Equation 37 is identical to the expression for the vertical downwash velocity at the 3/4 chord point of the foil.

An approximate form of the Wagner function was used in this analysis. The following are two approximations commonly used in aeronautical literature (reference 7).

$$\phi(s) \cong 1 - 0.165e^{-0.0455s} - 0.335e^{-0.3s} \tag{38}$$

or

$$\phi(s) \cong \frac{s + 2}{s + 4}. \tag{39}$$

The former was used because of its adaptability to the Laplace transform method of solution. Introducing these results into the equations of motion, taking the Laplace transform, and using the initial conditions (Figure 8),

$$h'(0) = \alpha'(0) = 0,\ h(0) = h_o \quad \text{and} \quad \alpha(0) = \alpha_o, \tag{40}$$

results in the following pair of simultaneous, linear, algebraic, nonhomogeneous equations in the transforms of the motion $\bar{h}(p)$ and $\bar{\alpha}(p)$ in which p is the complex Laplace transform variable:

$$\bar{h}\left\{p^2(\mu + 1 + 2\bar{\phi}) + \mu\Omega_h{}^2\right\} + \bar{\alpha}\left\{p^2\left[\mu\beta x_\alpha - a + 2(\tfrac{1}{2} - a)\bar{\phi}\right] + p(1 + 2\bar{\phi})\right\} = h_o p(\mu + 1 + 2\bar{\phi}) + \alpha_o\left\{1 + p\left[\mu\beta x_\alpha - a + 2(\tfrac{1}{2} - a)\bar{\phi}\right]\right\} \tag{41}$$

and

$$\bar{h}p^2\left\{\mu\beta x_\alpha - a - 2\left(\frac{1}{2}+a\right)\bar{\phi}\right\} + \bar{\alpha}\left\{p^2\left[\mu r_\alpha{}^2 + \frac{1}{8} + a^2 - 2\left(\frac{1}{4}-a^2\right)\bar{\phi}\right]\right.$$
$$\left. + p\left[\frac{1}{2} - a - 2\left(\frac{1}{2}+a\right)\bar{\phi}\right] + \mu r_\alpha{}^2\Omega_\alpha{}^2\right\} = h_o p\left[\mu\beta x_\alpha - a - 2\left(\frac{1}{2}+a\right)\bar{\phi}\right]$$
$$+ \alpha_o\left\{\frac{1}{2} - a + p\left[\mu r_\alpha{}^2 + \frac{1}{8} + a^2 - 2\left(\frac{1}{4}-a^2\right)\bar{\phi}\right]\right\}, \qquad (42)$$

where the bar indicates Laplace transformation. The transform of equation 38 yields

$$\bar{\phi}(p) = \frac{1}{p} - \frac{0.165}{p + 0.0455} - \frac{0.335}{p + 0.3} \qquad (43)$$

Finally, by solving equations 41 and 42 for the transformed responses $\bar{h}(p)$ and $\bar{\alpha}(p)$, then clearing the fraction yields

$$\bar{h}(p) = \frac{P(p)}{Q(p)} \quad \text{and} \quad \bar{\alpha}(p) = \frac{R(p)}{Q(p)} \qquad (44)$$

where P, Q and R are polynomials in p. P and R are of order five and Q is of order six, which permitted the following inverse transformation to be used:

$$\mathcal{L}^{-1}\ \frac{P(p)}{Q(p)} = \sum_{n=1}^{6} \frac{P(p_n)}{Q'(p_n)}\ e^{p_n s} \qquad (45)$$

where p_n are of the roots of the characteristic equation

$$Q(p) = 0 \qquad (46)$$

and where $Q'(p_n)$ is the derivative of $Q(p)$ with respect to p evaluated at $p = p_n$. These results may be confirmed in any textbook on operational methods (reference 11). An iterative process based on Newton's method was used to find the quadratic factors of equation 46 and is described in reference 12. The interest here lies in the complex roots of equation 46 and in particular the root in which the real part becomes positive above some critical speed. The results were obtained in the form of the overall damping ratio (σ/ω_α), which is the ratio of the real part of $-\lambda$ to the uncoupled rotational frequency. If the complex root of equation 46 is

$$p = u + i\,v \qquad (47)$$

then the overall damping ratio is found from the real part of p and the frequency ratio (ω/ω_α) from the imaginary part as follows

$$\frac{\sigma}{\omega_\alpha} = -\frac{u}{\Omega_\alpha} \; ; \quad \frac{\omega}{\omega_\alpha} = \frac{v}{\Omega_\alpha} \tag{48}$$

The overall damping ratio as predicted by this method for the experimental conditions is plotted in Figures 11 through 17 with the corresponding experimental results and the frequencies are presented in Figures 18 through 25.

C. CRITICAL DENSITY RATIO

An examination of the theoretical results, (particularly those shown in Figure 10) will show that the reduced flutter speed becomes infinite at some value of density ratio. This value can be predicted by using the following information: $U/b\omega_\alpha \rightarrow \infty$, when $k \rightarrow 0$ for finite values of ω/ω_α. An extension of the assumed modes analysis leads to an explicit equation for $U_F/b\omega_\alpha$ when these limits are introduced. This result is developed in reference 3, where the equation is shown to be a ratio of two polynomials. Setting the denominator of this result equal to zero yields the relation between the parameters that must be satisfied at the asymptote where $U_F/b\omega_\alpha \rightarrow \infty$ and $\mu = \mu_{CR}$, the critical density ratio. It is found that μ_{CR} decreases with ω_h/ω_α and a very simple relation is found for the limiting case $\omega_h/\omega_\alpha = 0$,

$$\mu_{CR} = \frac{1}{2(x_\alpha + a) + 1} \tag{49}$$

where $x_\alpha + a$ is the c.g. location measured in half-chord lengths from midchord, positive if the c.g. is aft. This result is plotted in Figure 25.

By this procedure, an asymptotic behavior is predicted for the flutter speed as μ approaches μ_{CR}. However, this asymtote is approached from the low μ side in many cases so that μ_{CR} is not always the minimum density ratio at which flutter is predicted.

IV. DISCUSSION

A. GENERAL

In these experiments, flutter was induced under controlled and somewhat artificial conditions to validate the application of airfoil theory to hydrofoil phenomena. Consequently, these theoretical studies were carried out in accordance with aeronautical practices.

B. EXPERIMENTAL PROCEDURE

At each mass condition (μ_n, where n = 0, 1, 2, 4, 7, 9, 11) two bits of experimental information were obtained; the overall damping ratio (σ/ω_α), and the frequency ratio (ω/ω_α). The model was locked in position and when the apparatus attained the desired speed, the model was released and the resulting motion was recorded. The speed of each successive test was increased until the motion of the model was divergent, in which case the apparatus was quickly brought to rest to avoid destructive or violent motions. Flutter was obtained in each test series except series 0 ($\mu = 0.758$).

A time signal was recorded simultaneously with the motions to measure frequency (ω). Because the model had two degrees of freedom, two values of ω were obtainable. The coupled zero-speed, rotation mode-shape led to flutter. The damping in the translation mode increased rapidly with speed, conveniently aiding its elimination from the records. By properly choosing initial conditions, appreciable response in the translation mode was eliminated.

The second piece of information, the overall damping ratio (σ/ω_α), was obtained using

$$\frac{\sigma}{\omega_\alpha} = -\frac{1}{2\pi}\left(\frac{\omega}{\omega_\alpha}\right)\left[\frac{\ell n}{i}\left(\frac{\alpha_{o_1} + i}{\alpha_{o_1}}\right)\right], \qquad (49)$$

where i is the number of cycles analyzed. The quantity in square brackets is proportional to the slope of a straight line faired through the successive amplitudes of oscillation plotted on semi-log graph paper.

The tests were performed in two groups (series 4, 7, 11 and series 0, 1, 2, 9, respectively), separated by two weeks, during which time, some of the data were analyzed. During this time it was realized that the rotation mode of vibration was leading to flutter; subsequently, the model was held at an initial angle of attack rather than with an initial translation displacement, as in the first group of tests. During the second group of tests, an investigation of the effect of initial conditions on the experimental measurements showed that the results of the first group could still be used, because of the large amount of damping in the translation mode of vibration; by repeated runs at a particular speed, the results were found to be reproducible. (See points at $U/b\omega_\alpha = 1.11$ in Figure 14 or at $U/b\omega_\alpha = 1.21$ in Figure 17.)

C. EXPERIMENTAL RESULTS

The maximum speed obtainable was considerably lower than anticipated. The apparatus was designed on the basis of a maximum speed of 30 feet per second. Actually, this speed was 15 feet per second ($U/b\omega_\alpha = 1.67$, for series 0, $\mu = 0.758$, where the limitation was most severe and the only mass condition in which the maximum speed was obtained). The experimental results for the present investigation are somewhat inconclusive in this regard: it is not certain that flutter could not be induced at a higher speed for series 0 (Figure 11). However, a sharp upward turn in reduced flutter speed does occur as μ decreases, (Figure 10), which at least partially substantiates the existance of an asymptote as predicted.

D. THEORETICAL RESULTS

The analysis by the two theoretical methods that can be used to predict speed and frequency at flutter has shown that (1) the assumed modes method of flutter analysis leads to a prediction of μ_{CR} at which the flutter speed increases asymptotically and (2) the superposition method of stability analysis provides information for speeds other than the flutter speed; these results were obtained in addition to the prediction of critical flutter-speed and frequency.

The flutter speeds as predicted by the assumed modes analysis, which involved an exact modal description in this case, are shown in Figure 10 and the corresponding frequencies for each test condition are shown in Table II. The critical-density ratio as predicted by this analysis at $\omega_h/\omega_\alpha = 0$ is plotted in Figure 25. The difference between series 0, 1, 2, 9 and series 4, 7, 11 (Figure 10) is caused by the change in x_α between these two groups, thus causing a slight shift in μ_{CR}.

Figures 11 through 17 show the overall damping ratio obtained from the superposition analysis, which reduces to the well-known critical damping ratio for a one-degree of freedom system vibrating freely in air, plotted against the reduced speed for each mass condition. The predicted flutter speed is found where σ/ω_α goes to zero. A comparison of these speeds with the theoretical results from the assumed modes analysis in Figure 10 for corresponding μ's shows the anticipated identical agreement between the two methods. The use of the approximation in equation 38, thus agrees well with more exact theory. No flutter is predicted for series 0 or 1. Figures 18 through 24 show the frequency ratio versus reduced speed, as predicted by the superposition method.

Other results of the superposition analysis are tabulated in Table III for series 9 ($\mu = 3.03$).

The theoretical results described here were obtained on an electronic digital computer. The program for both the assumed modes and the superposition analysis have been retained for future use.

V. THEORY COMPARED WITH EXPERIMENT

The results of series 7, 9, and 11 show relatively good agreement between theory and experiment for the predicted flutter conditions (Table II). As cited in reference 4 and as indicated in Figure 10, the theory gave a conservative estimate of flutter speed for these conditions. No apparent reason could be found to doubt the results of series 7 (μ = 2.06) in Figure 10; however, there is nothing to cause these results to be out of line with the other series. A lower experimental value for the reduced flutter speed at this mass condition would be in agreement with the anticipated experimental results.

Between series 7 and 4, the inadequacy of the theory to predict the flutter speed with accuracy becomes more apparent and the resulting error becomes more dangerous. Although the good agreement in frequency ratio is retained at the lower density ratios, the overall damping ratio is considerably overestimated by the theory; in fact, at series 1 the theory predicts freedom from flutter where flutter was obtained during the experiments. In the case of series 0, flutter, though it did not occur, was imminent; the theory predicts no flutter at all speeds. Even in this circumstance the frequency ratio is well predicted (Figure 18) and is within 9 percent.

The results of reference 4, indicated a discrepancy between theory and experiment for the prediction of flutter speed at low density ratios. However, they were not able to extend their investigations to a sufficiently low value of density ratio to check the existence of an asymptote as predicted by equation 49. These results are summarized in Figure 1. At high values of density ratio (μ = 3.0) the

theoretical and experimental results were essentially in agreement, or the theory was conservative.

The present results shown in Figure 10 substantiate the results of reference 4. In addition, the experimental results at series 0(μ = 0.758) strongly indicate the existence of an asymptote in flutter speed. There is definitely a sharp upward trend shown as μ decreases. The position of this asymptote is not correctly predicted by theory. The theoretical and experimental value of μ_{CR} are plotted in Figure 25. The comparison is somewhat worse than is shown there since the theoretical curve is derived for the case $\omega_h/\omega_\alpha = 0$ and in reference 3, it is shown that μ_{CR} increases with ω_h/ω_α.

Some more definite information about the discrepancy can be gotten from the results of the stability analysis. The experimental and theoretical overall damping ratios are compared in Figures 11 through 17. There, it is seen that σ/ω_α is overestimated by the theory up to series 7 (μ = 2.08) and from that point on the predicted overall damping ratio is less than that obtained in the experiments. The frequency ratio is very well predicted throughout as shown in Figures 18 through 24. We have found that the frequency ratio depends mainly on terms proportional to h(t) and α(t) or their second derivatives; however, the damping ratio depends mostly on terms proportional to the first derivatives. The latter contain the circulatory responses--that is, the Theodorsen or Wagner functions; the former are not as sensitive to these functions. Since the frequency ratio is fairly well predicted and the damping is not, it may be surmised that the effective mass and inertia terms in the theory are more accurate than the circulatory terms. Other investigators have used this hypothesis as mentioned in reference 3.

VI. CONCLUSIONS

1. A conservative prediction of flutter speed may be expected at high-density ratios.

2. The theory does not correctly predict the flutter speed near μ_{CR}.

3. The theory does not correctly predict the location of μ_{CR}.

4. The frequency is very well predicted at flutter and at lower speeds at all density ratios.

5. The overall damping ratio does not agree with experimental results.

6. The circulatory terms in the theory are more liable to doubt than the effective mass or spring terms.

VII. RECOMMENDATIONS

Further investigations are in order to describe more fully the discrepancy that has been shown to exist. Several different values of c.g. location and radius of gyration should be used in further investigations. In addition to the results presented here, an experimental determination of amplitude ratio and phase angle should be attempted. Single degree of freedom studies in water should be carried out, to provide separate comparisons between theory and experiment for each component of the lift and moment expressions. Also, zero-speed responses must be analyzed to check the prediction of added mass, added inertia, and added mass coupling terms.

VIII. REFERENCES

1. Jewell, D. A.: "A Note on Hydroelasticity," Journal of Ship Research, Vol. 3, No. 4, pp. 9-12, March 1960.

2. Abramson, H. N. and Chu, Wen-Hwa, "A Discussion of the Flutter of Submerged Hydrofoils," Journal of Ship Research, Vol. 3, No. 2, pp. 5-13, October 1959.

3. Henry, C. J., Dugundji, J., and Ashley, H.: "Aeroelastic Stability of Lifting Surfaces in High Density Fluids," Journal of Ship Research, Vol. 2, No. 4, pp. 10-21, March 1959.

4. Woolston, D. S. and Castile, G. E.: "Some Effects of Variations in Several Parameters Including Fluid Density on the Flutter Speed of Light Uniform Cantilever Wings," NACA TN 2558, 1951.

5. McGoldrick, R. T.: "Rudder Excited Hull Vibrations on USS Forest Sheridan (DD 931)...(A Problem in Hydroelasticity)," Transactions of The Society of Naval Architects and Marine Engineers, Vol. 67, pp. 341-385, 1959.

6. Abbott, I. A. and Von Doenhoff, A. E.: "Theory of Wing Sections," Dover Publications, Inc., New York, 1959.

7. Bisplinghoff, R. L., Ashley, H., and Halfman, R. L.: "Aeroelasticity," Addison-Wesley Publishing Co., Reading, Mass, 1955.

8. Theodorsen, T.: "General Theory of Aerodynamic Instability and the Mechanism of Flutter," NACA Report 496, 1935.

9. Smilg, B. and Wasserman, L. S.: "Application of Three Dimensional Flutter Theory to Aircraft Structures," Air Force Technical Report 4798, 1942.

10. Scanlan, R. H. and Rosenbaum, R.: "Aircraft Vibration and Flutter," the MacMillan Co., New York, 1951.

11. Churchhill, R. V.: "Operational Mathematics," McGraw-Hill, New York, 1958.

12. Scarborough, J. B.: "Numerical Mathematical Analysis," The Johns Hopkins Press, Baltimore, 1950.

TABLE I

PROPERTIES OF MODEL TENITE II, FORMULA 233, FLOW MS

Flow Temperature	284°F
Specific Gravity	1.22
Modulus of Elasticity	1.30×10^5 psi
Deformation under Load (Cold Flow)	33%
Water Absorption (24 Hrs. Immersion)	
Total Weight Gained	1.3%
Soluble Matter Lost	0.1%
Accelerated Aging Weight Lost (72 hrs at 180°F)	1.6%

TABLE II

PARAMETERS AND FLUTTER CONDITIONS

Series No.	μ	x_α	r_α^2	$(\frac{\omega_h}{\omega_\alpha})^2$	$U_F/b\omega_\alpha$ exp.	$U_F/b\omega_\alpha$ the.	ω_F/ω_α exp.	ω_F/ω_α the.	$m \times 10^3$ $\frac{lb\ sec^2}{in^2}$	ω_α $\frac{rad}{sec}$
0	.758	.496	.900	.251	--	--	--	--	2.00	36.0
1	.883	.496	.895	.264	1.22	--	.960	--	2.33	32.3
2	1.008	.496	.891	.260	1.14	1.84	.970	1.000	2.66	30.2
4	1.285	.465	.862	.269	1.08	1.42	.980	.977	3.39	26.8
7	2.06	.465	.839	.277	1.53	1.29	.910	1.002	5.43	21.3
9	3.03	.496	.868	.258	1.44	1.32	.980	1.040	8.00	17.5
11	4.07	.465	.895	.268	1.55	1.45	.985	1.020	10.74	15.0

b = 3 inches, a = -0.5

TABLE III

TYPICAL RESULTS FROM SUPERPOSITION CALCULATION

Series 9, $a = -0.5$, $x_\alpha = 0.496$, $r_\alpha^2 = 0.868$, $(\omega_h/\omega_\alpha)^2 = 0.258$, $\mu = 3.03$

	λ_1, λ_2				λ_3, λ_4				λ_5	λ_6
$U/b\omega_\alpha$	σ/ω_α	ω/ω_α	$\lvert h/\alpha \rvert$	ϕ	σ/ω_α	ω/ω_α	$\lvert h/\alpha \rvert$	ϕ	u_1	u_2
0.01	.00044	1.192	.576	179.6°	.00143	.423	5.84	- .370°	-.0455	-.300
0.26	.01129	1.186	.573	170.8°	.0380	.427	5.64	- 9.80°	-.0454	-.295
0.51	.0208	1.169	.568	161.1°	.0795	.439	5.08	- 20.12°	-.0453	-.281
0.76	.0270	1.141	.563	149.6°	.1310	.460	4.25	- 32.2°	-.0450	-.259
1.01	.0258	1.099	.574	134.8°	.1993	.491	3.24	- 47.1°	-.0445	-.229
1.26	.00874	1.045	.652	116.8°	.295	.535	2.25	- 67.1°	-.0438	-.1940
1.51	-.0325	.992	.868	103.0°	.424	.583	1.563	- 94.0°	-.0429	-.1576
1.76	-.0869	.956	1.182	98.8°	.572	.622	1.246	-121.1°	-.0416	-.1264
2.01	-.1399	.933	1.505	99.5°	.719	.655	1.107	-141.6°	-.0399	-.1031
2.26	-.1884	.916	1.811	101.6°	.861	.686	1.029	-156.1°	-.0376	-.0869
2.51	-.233	.901	2.10	104.1°	.997	.717	.976	-166.4°	-.0348	-.0762
2.76	-.275	.886	2.38	106.7°	1.129	.750	.936	-174.1°	-.0316	-.0692
3.01	-.315	.872	2.65	109.3°	1.258	.783	.903	-180.0°	-.0284	-.0648

REGION 1 a) NO FLUTTER

b) NO FLUTTER THEORETICALLY, NO EXPERIMENTAL INFORMATION

REGION 2 FLUTTER FOUND EXPERIMENTALLY, BUT NONE PREDICTED

REGION 3 THEORY PREDICTS FLUTTER AT HIGHER SPEED THAN THAT FOUND IN EXPERIMENTS

REGION 4 THEORY GIVES CONSERVATIVE PREDICTION OF FLUTTER SPEED

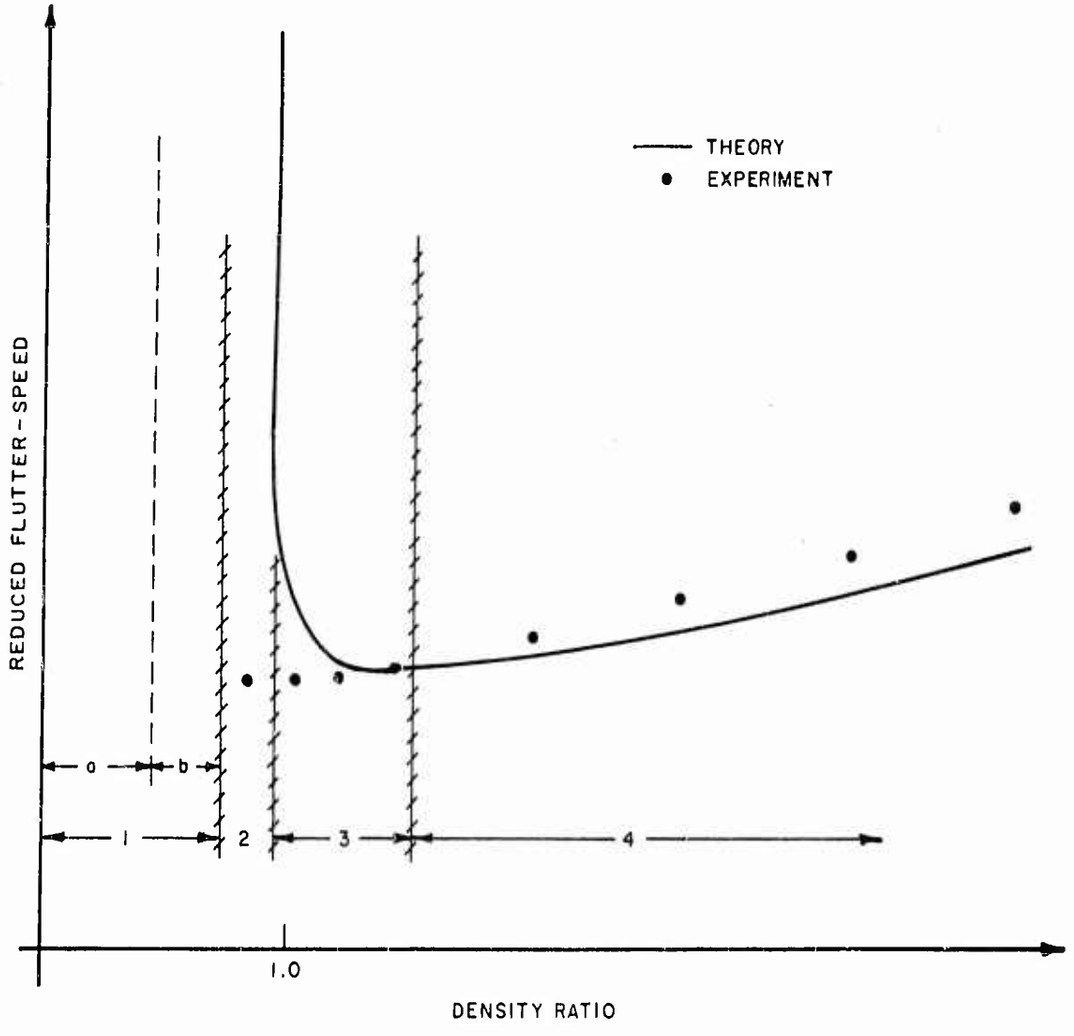

FIGURE 1. PREVIOUS EXPERIMENTAL RESULTS

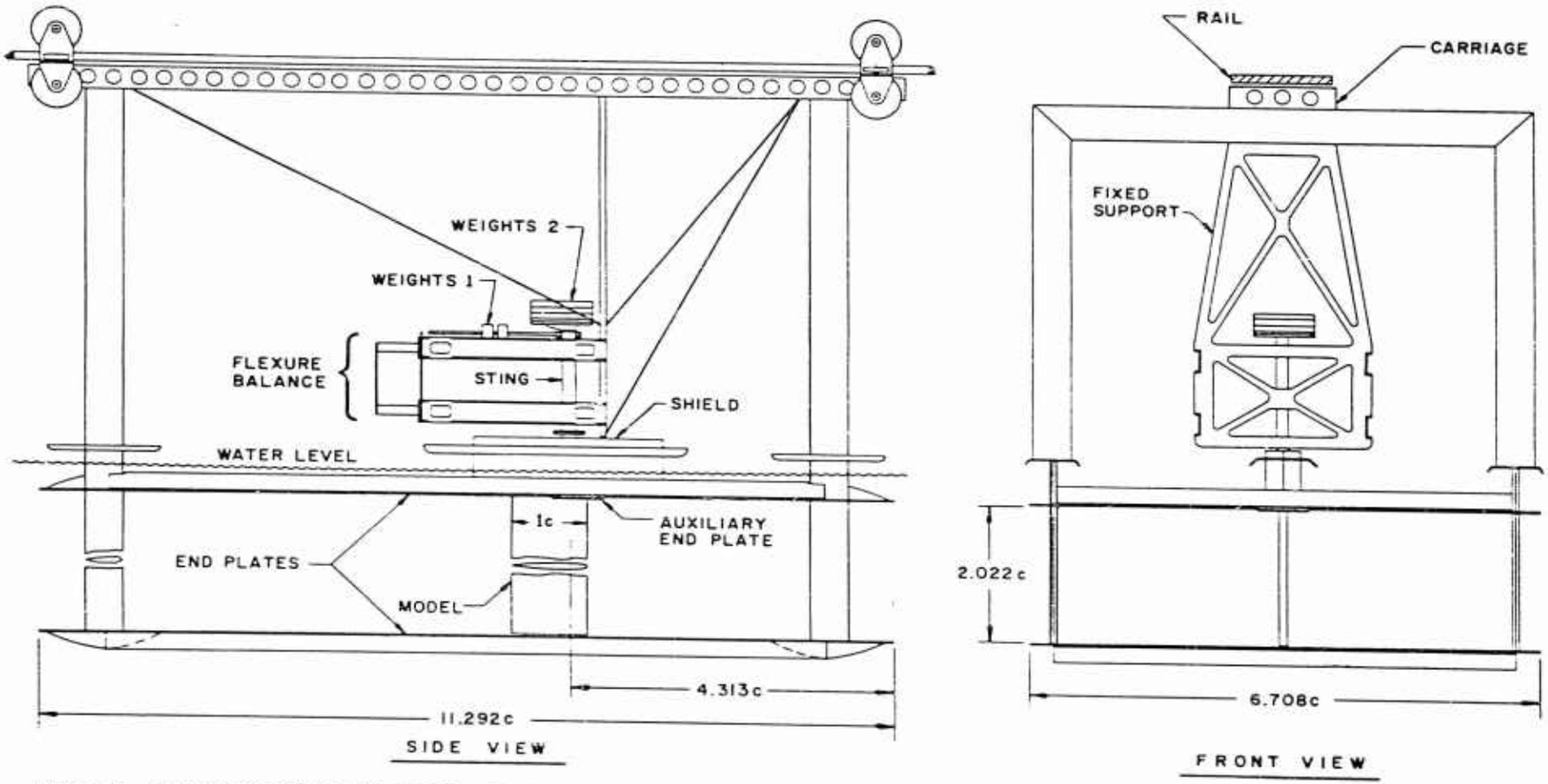

NOTE: 1 DIMENSIONS GIVEN IN CHORD LENGTHS, c = 6 inches
2 MAXIMUM CLEARANCE AT EACH END OF MODEL 0.006c

FIGURE 2. TEST APPARATUS

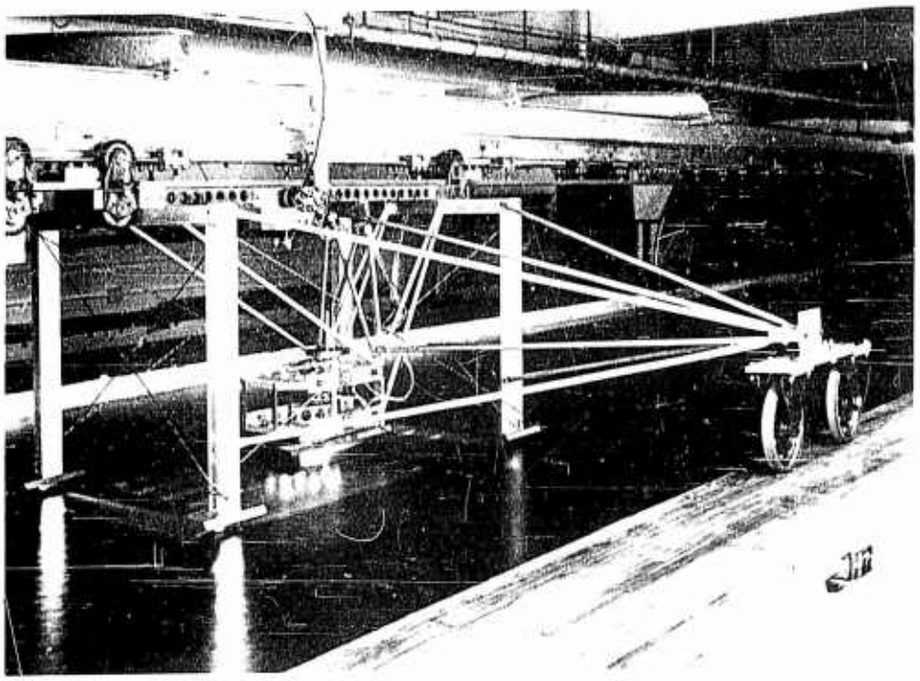

FIGURE 3. APPARATUS, STARBOARD SIDE

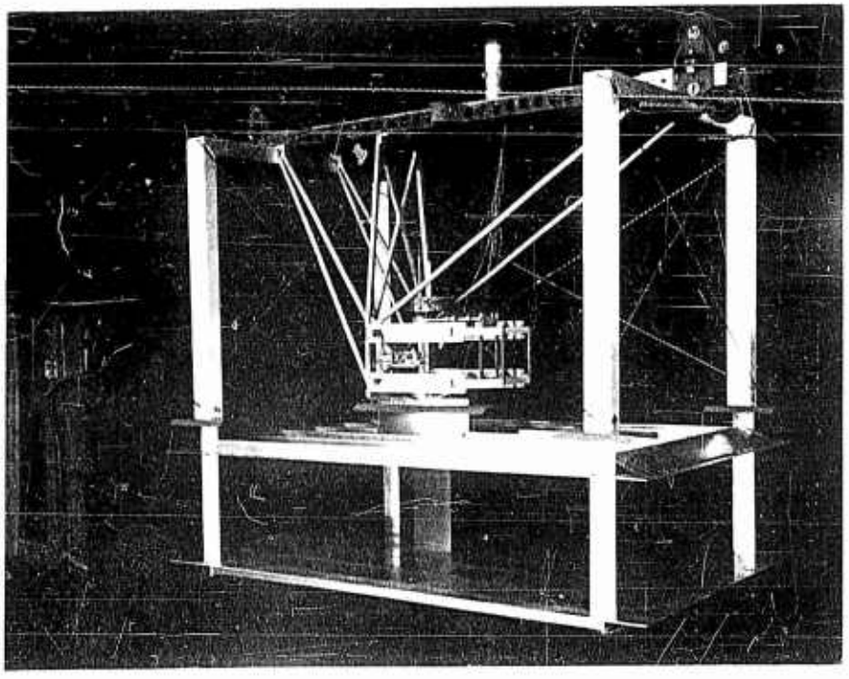

FIGURE 4. APPARATUS, PORT SIDE

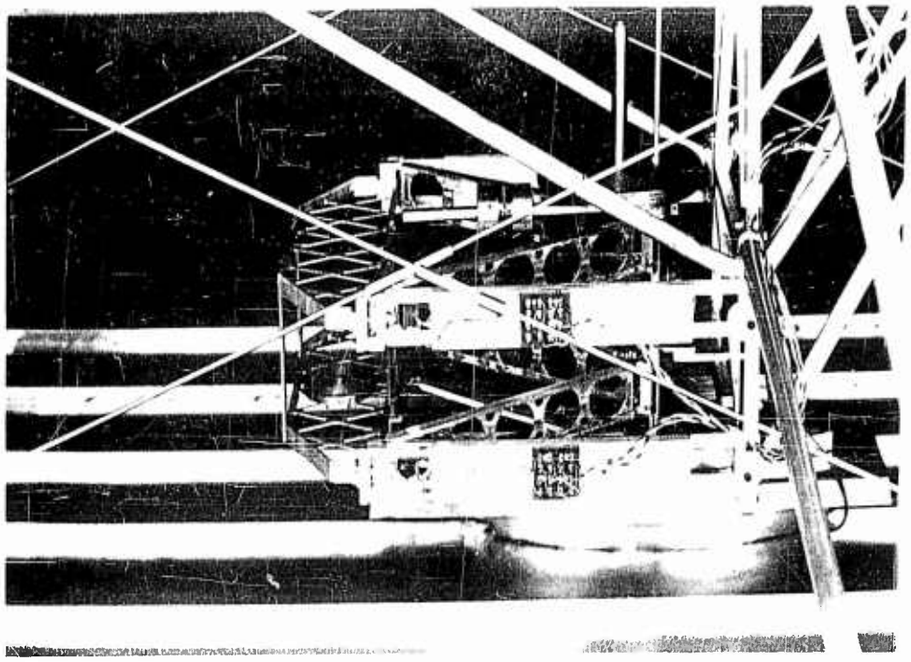

FIGURE 5. BALANCE, STARBOARD SIDE

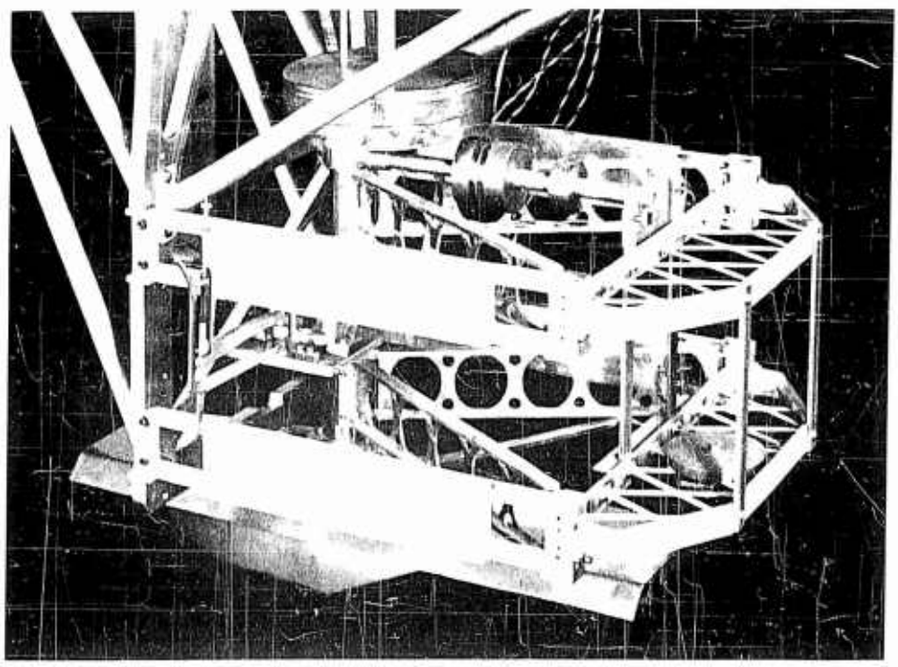

FIGURE 6. BALANCE, PORT SIDE

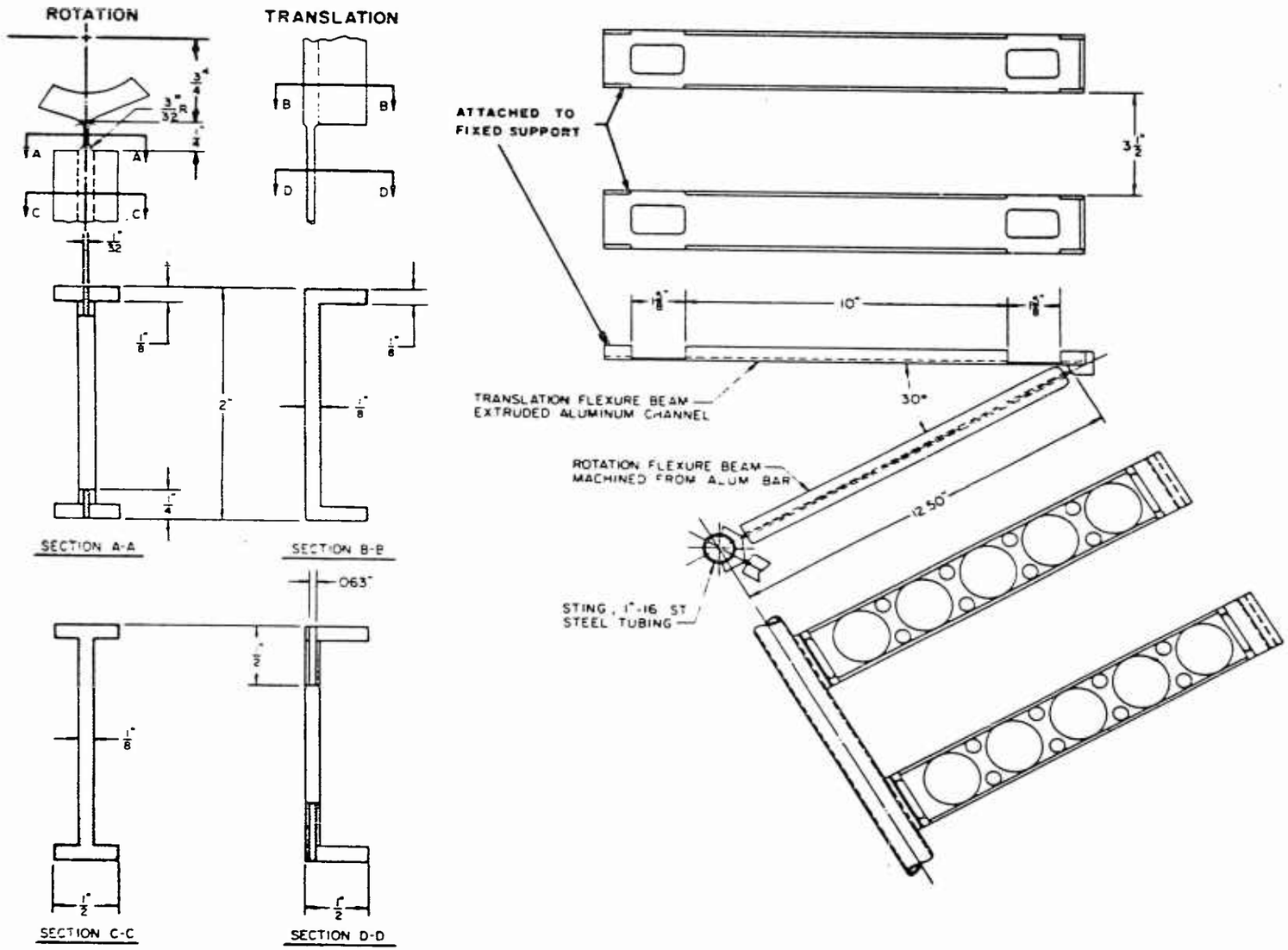

FIGURE 7. FLEXURE BALANCE

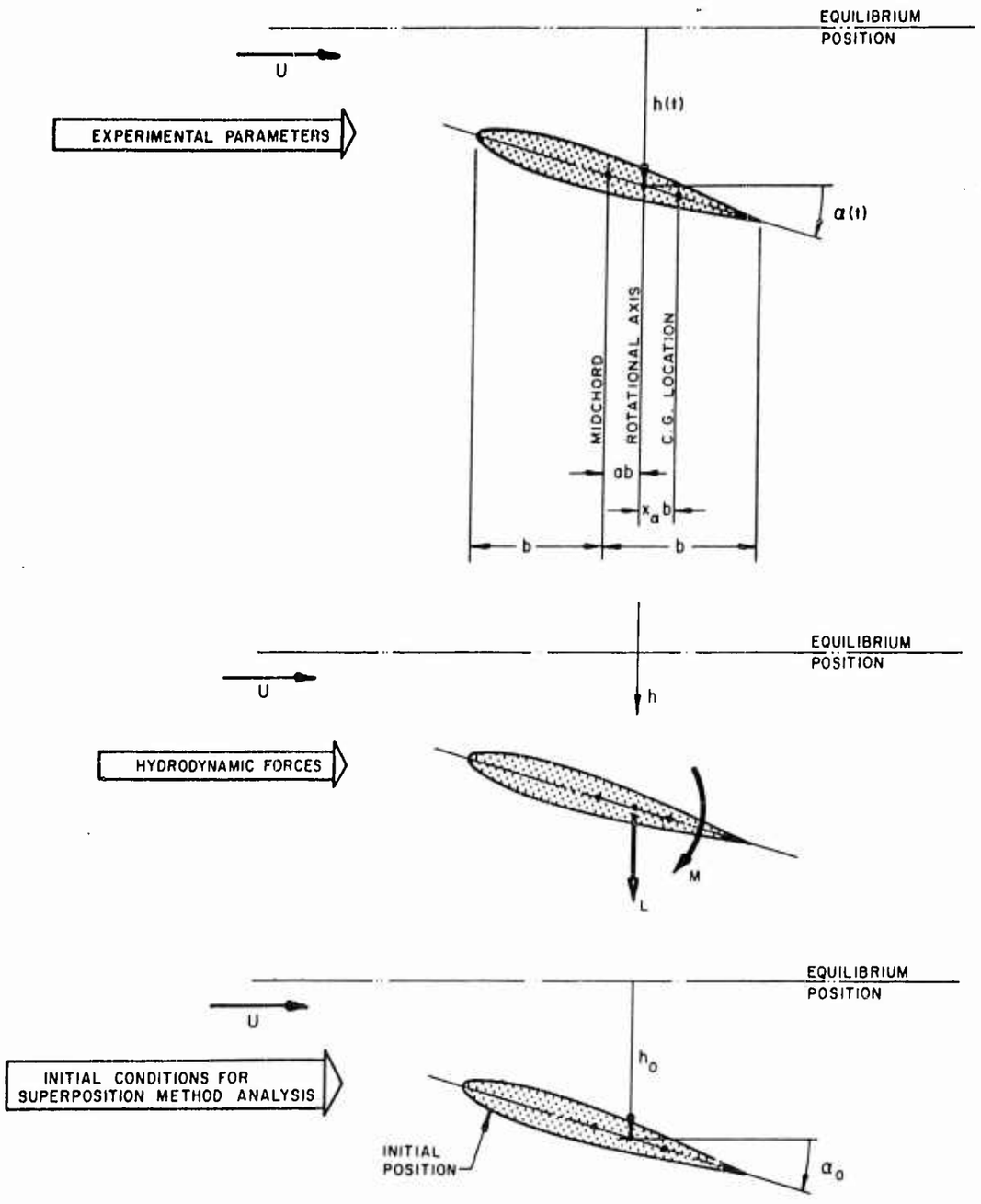

$$h(0) = h_o b \,,\ \alpha(0) = \alpha_o$$

$$\dot{h}(0) = \dot{\alpha}(0) = 0$$

FIGURE 8. REPRESENTATIVE HYDROFOIL ORIENTATION FOR THEORETICAL ANALYSIS

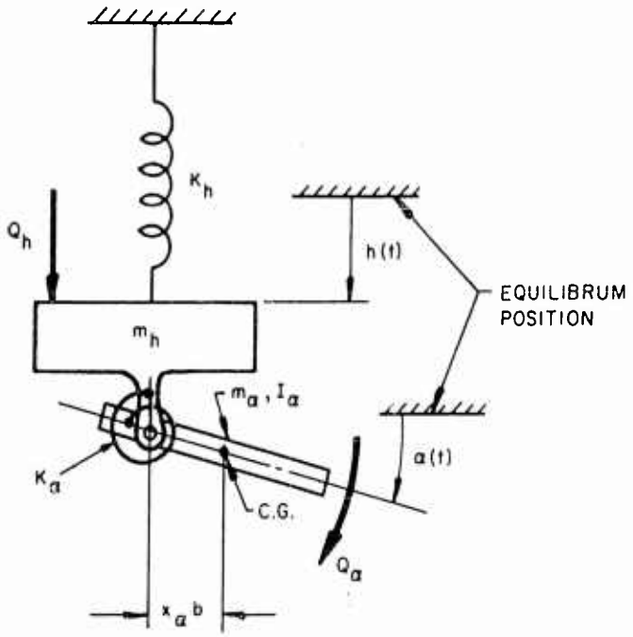

FIGURE 9. SCHEMATIC DIAGRAM OF SYSTEM USED FOR DYNAMIC ANALYSIS

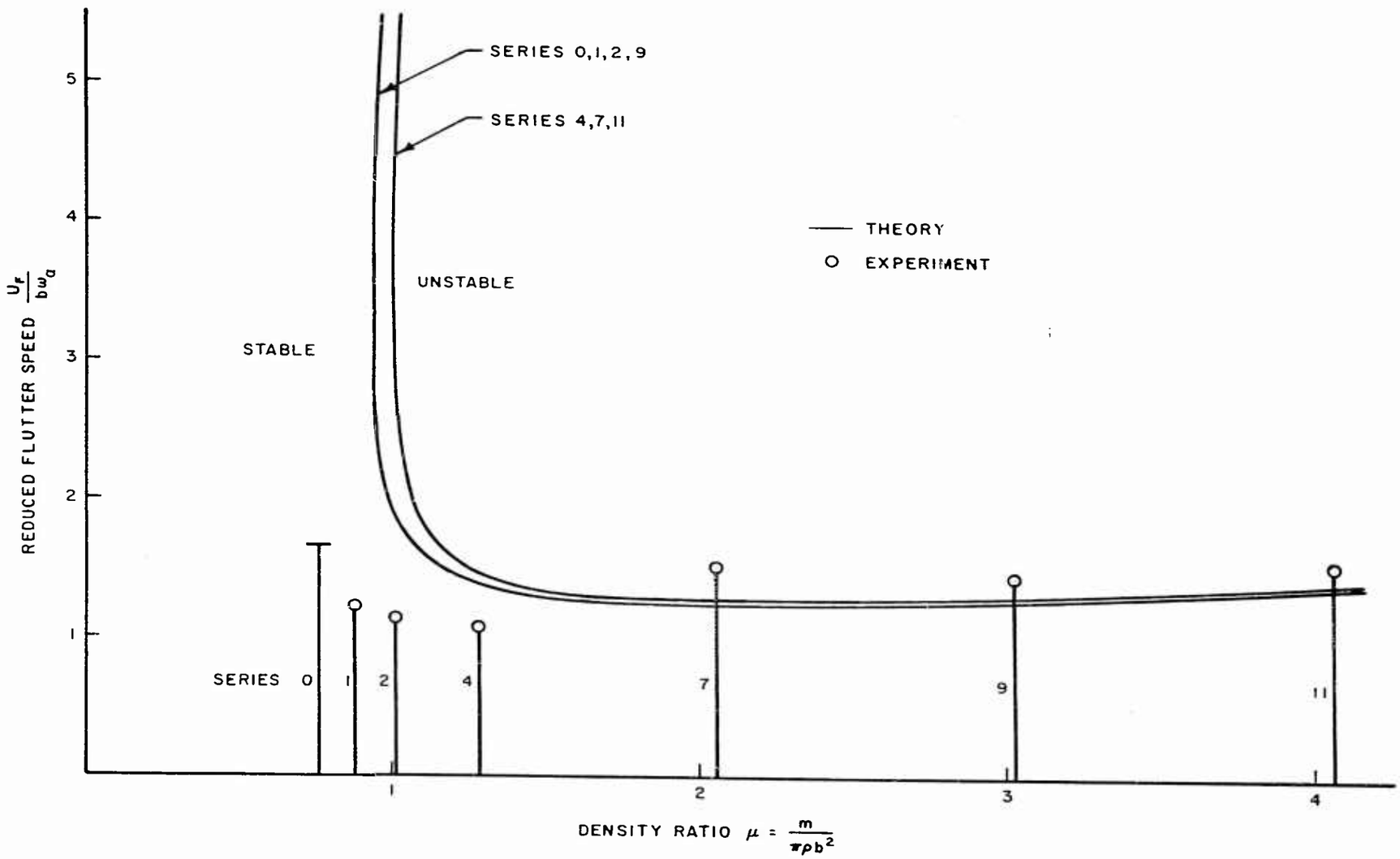

FIGURE 10. REDUCED FLUTTER-SPEED VERSUS DENSITY RATIO

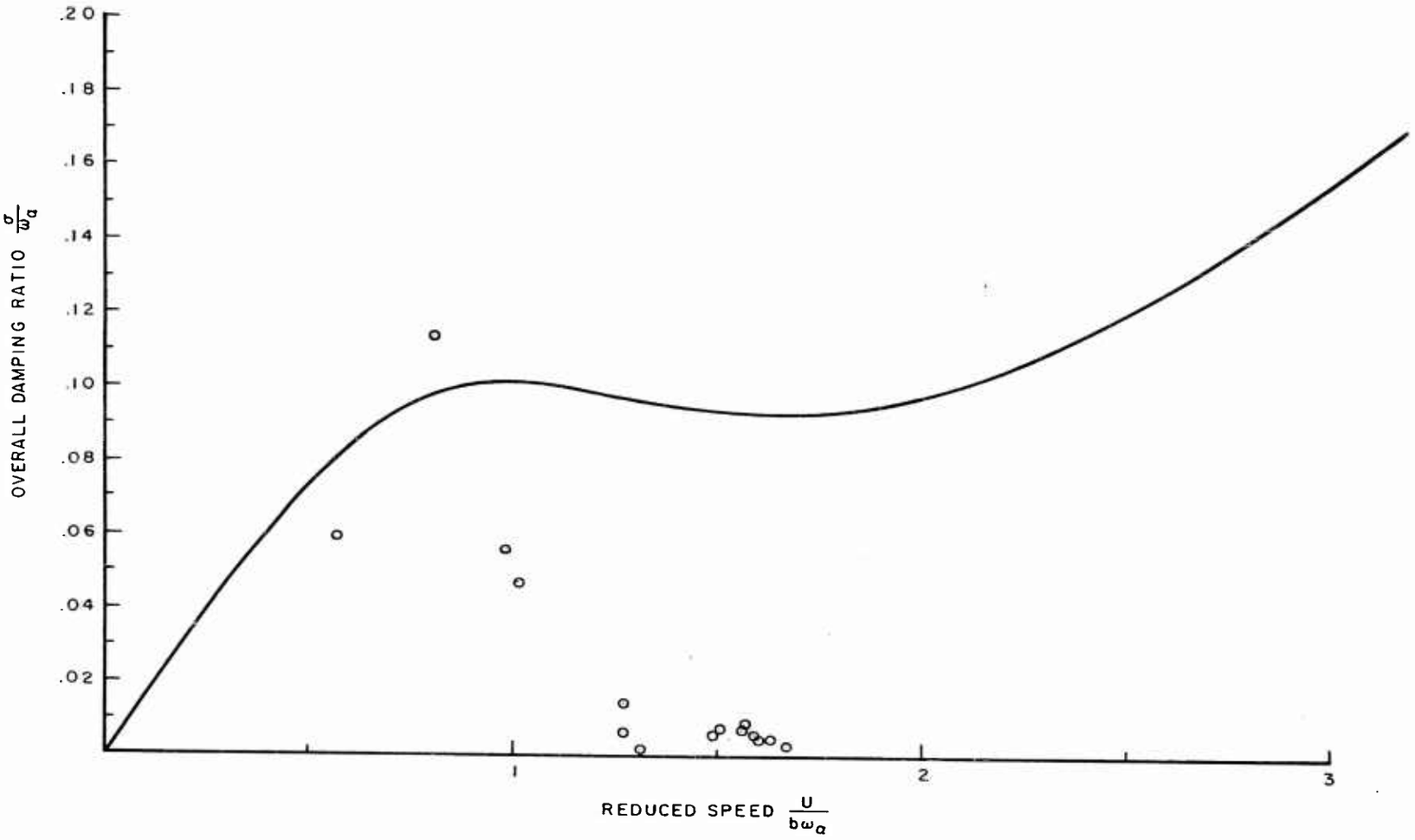

FIGURE 11. OVERALL DAMPING RATIO VERSUS REDUCED SPEED (STABILITY ANALYSIS, SERIES 0, μ = 0.758)

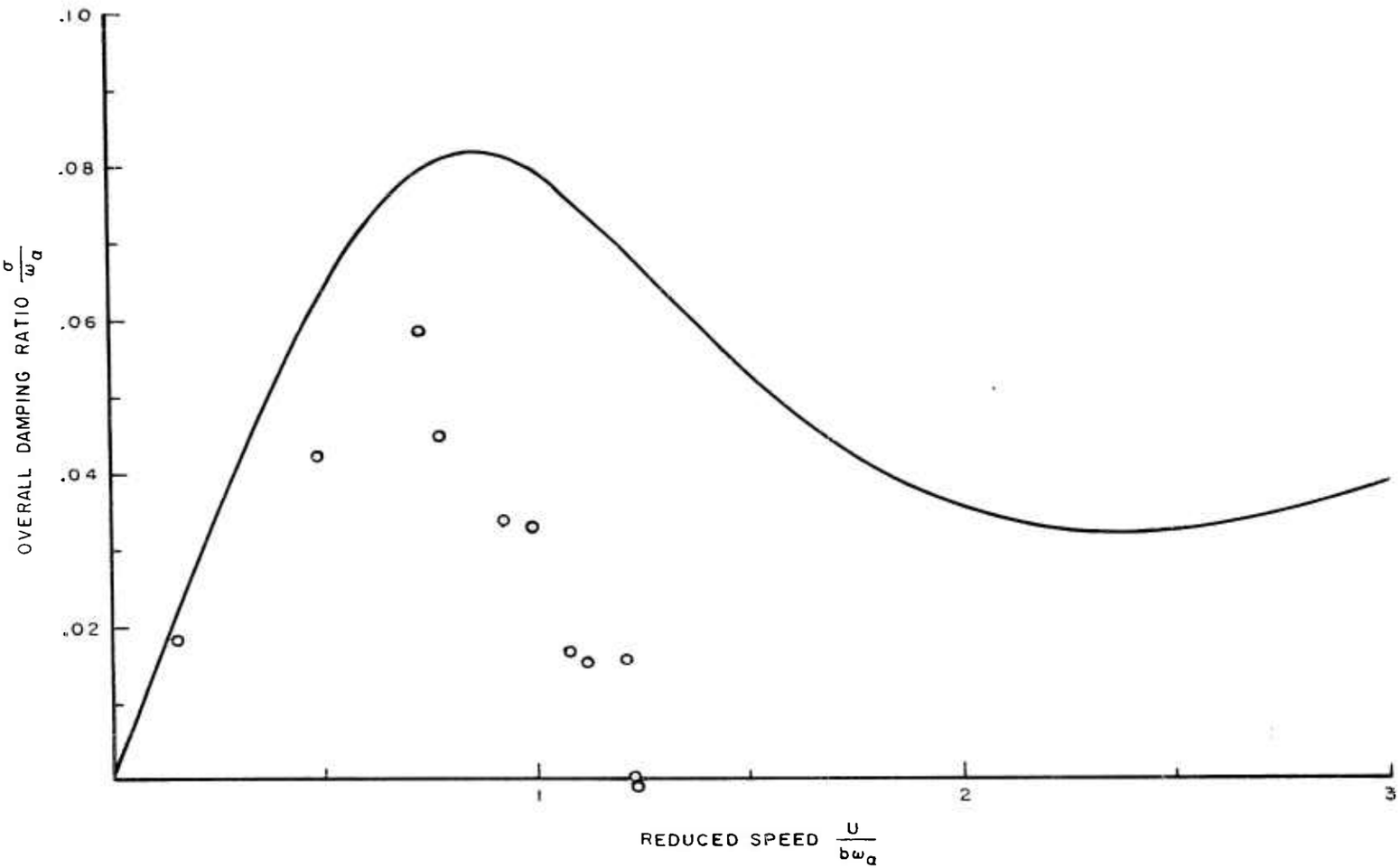

FIGURE 12. OVERALL DAMPING RATIO VERSUS REDUCED SPEED (STABILITY ANALYSIS, SERIES I, μ = 0.883)

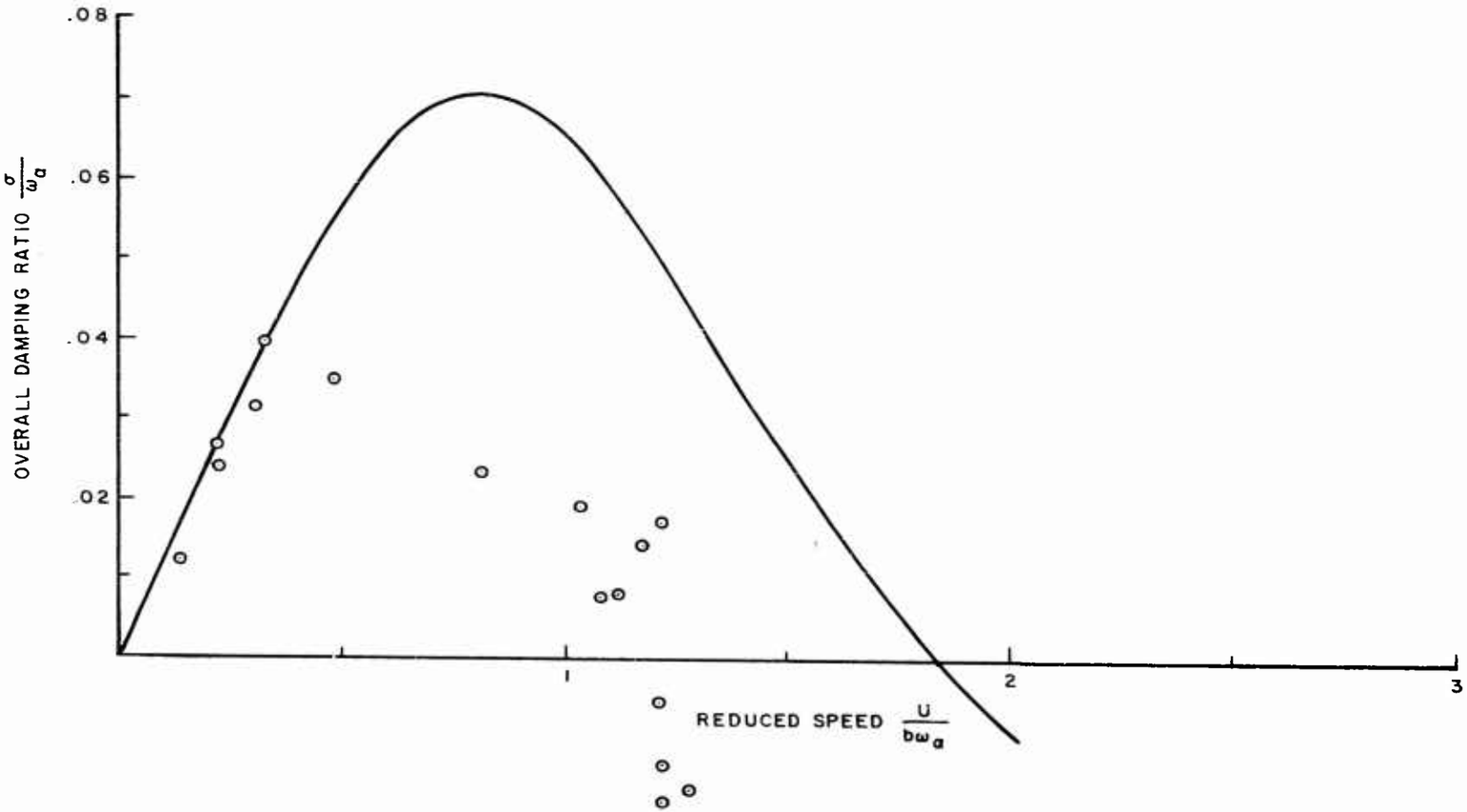

FIGURE 13. OVERALL DAMPING RATIO VERSUS REDUCED SPEED (STABILITY ANALYSIS, SERIES 2, μ = 1.008)

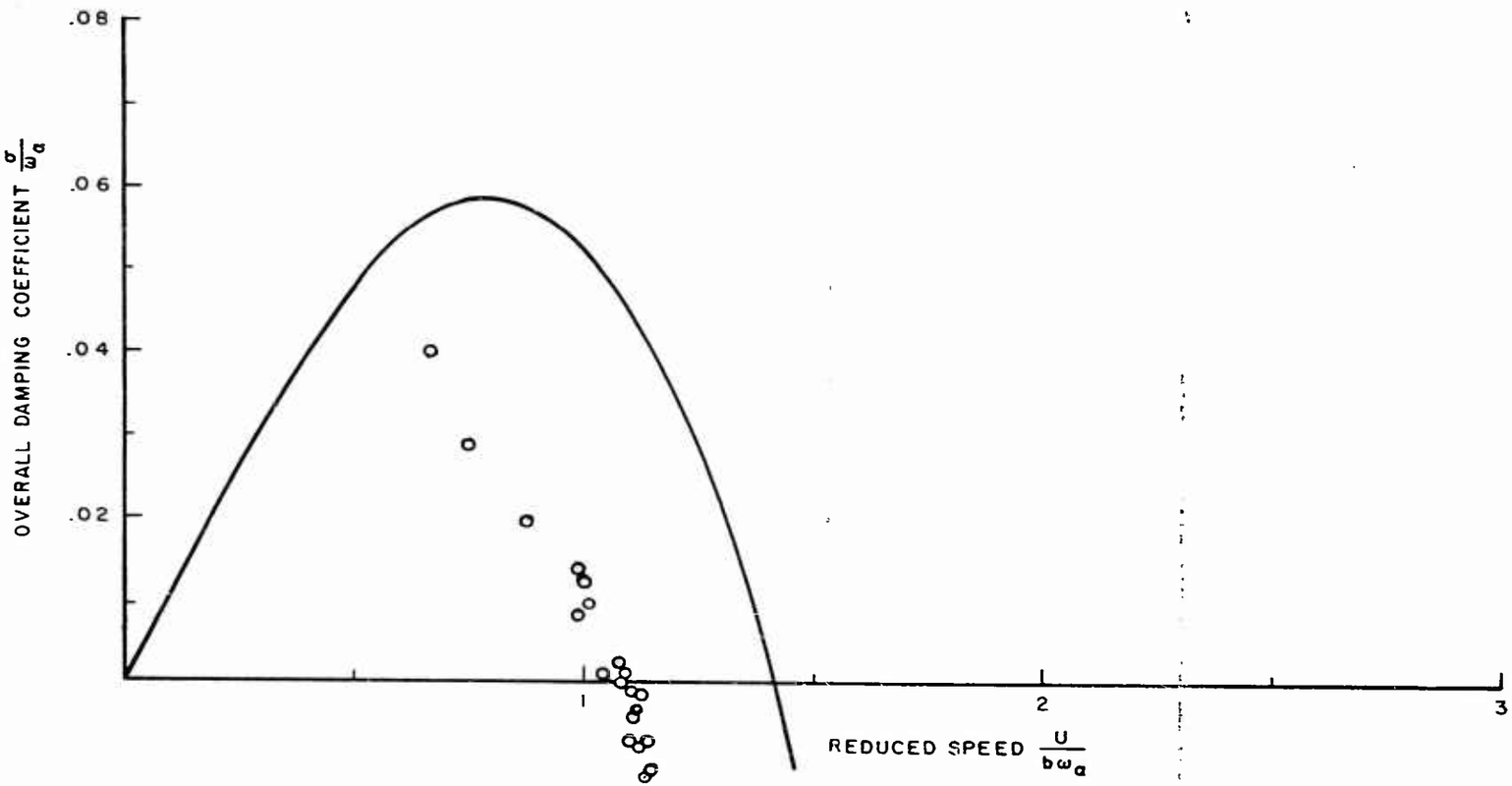

FIGURE 14. OVERALL DAMPING COEFFICIENT VERSUS REDUCED SPEED (STABILITY ANALYSIS, SERIES 4, μ = 1.285)

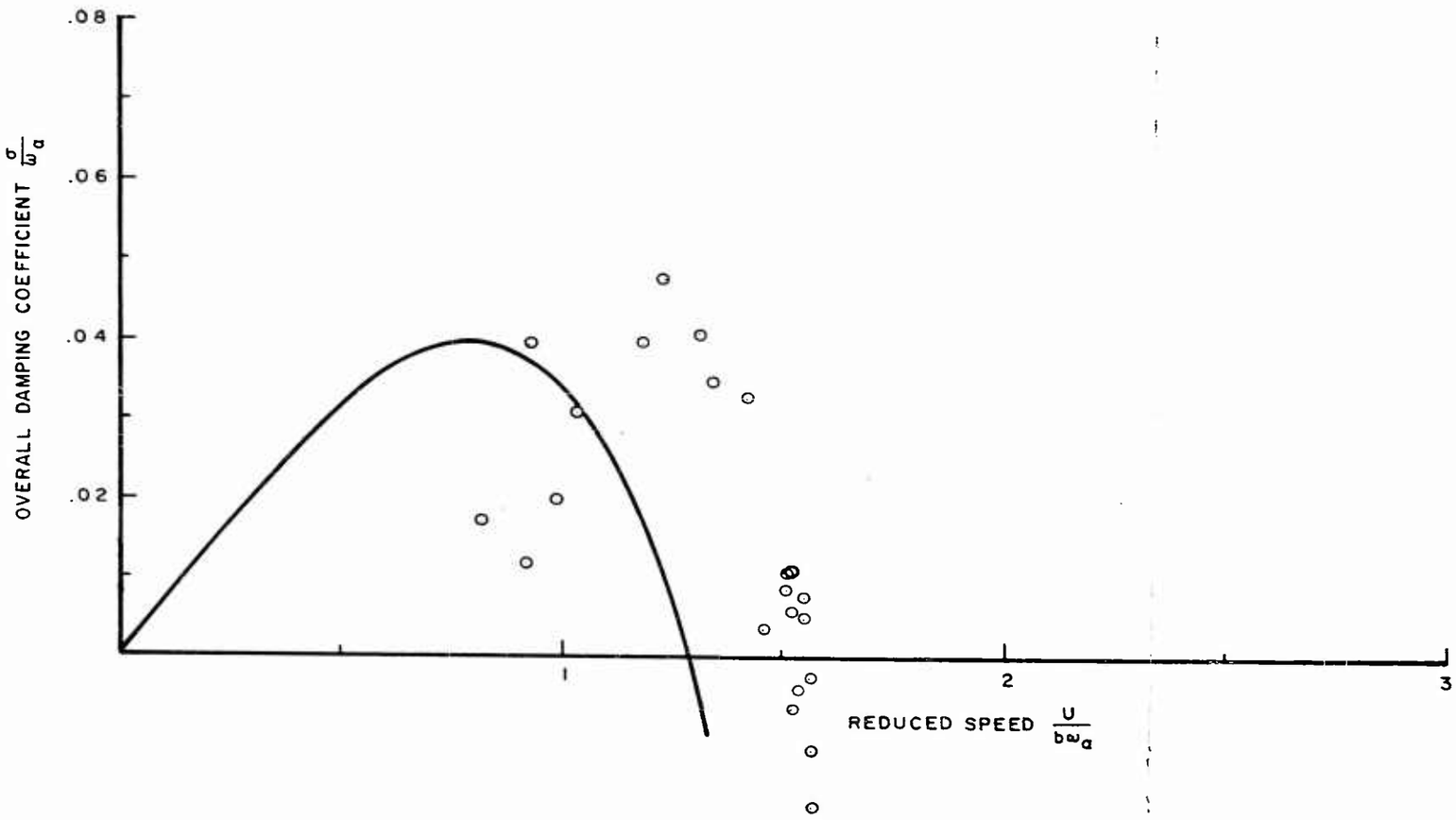

FIGURE 15. OVERALL DAMPING COEFFICIENT VERSUS REDUCED SPEED (STABILITY ANALYSIS, SERIES 7, μ = 2.08)

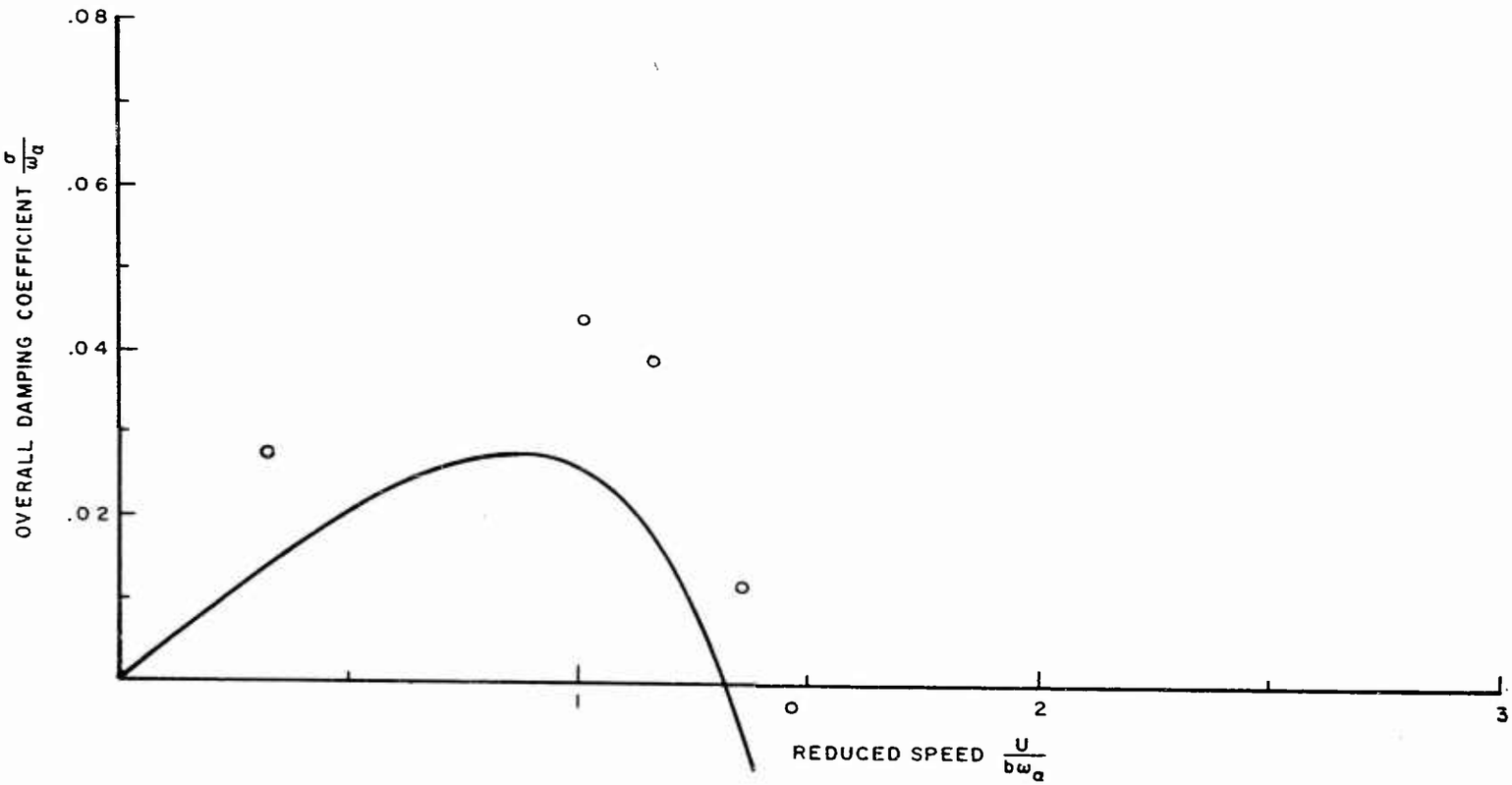

FIGURE 16. OVERALL DAMPING RATIO VERSUS REDUCED SPEED (STABILITY ANALYSIS, SERIES 9, μ = 3.03)

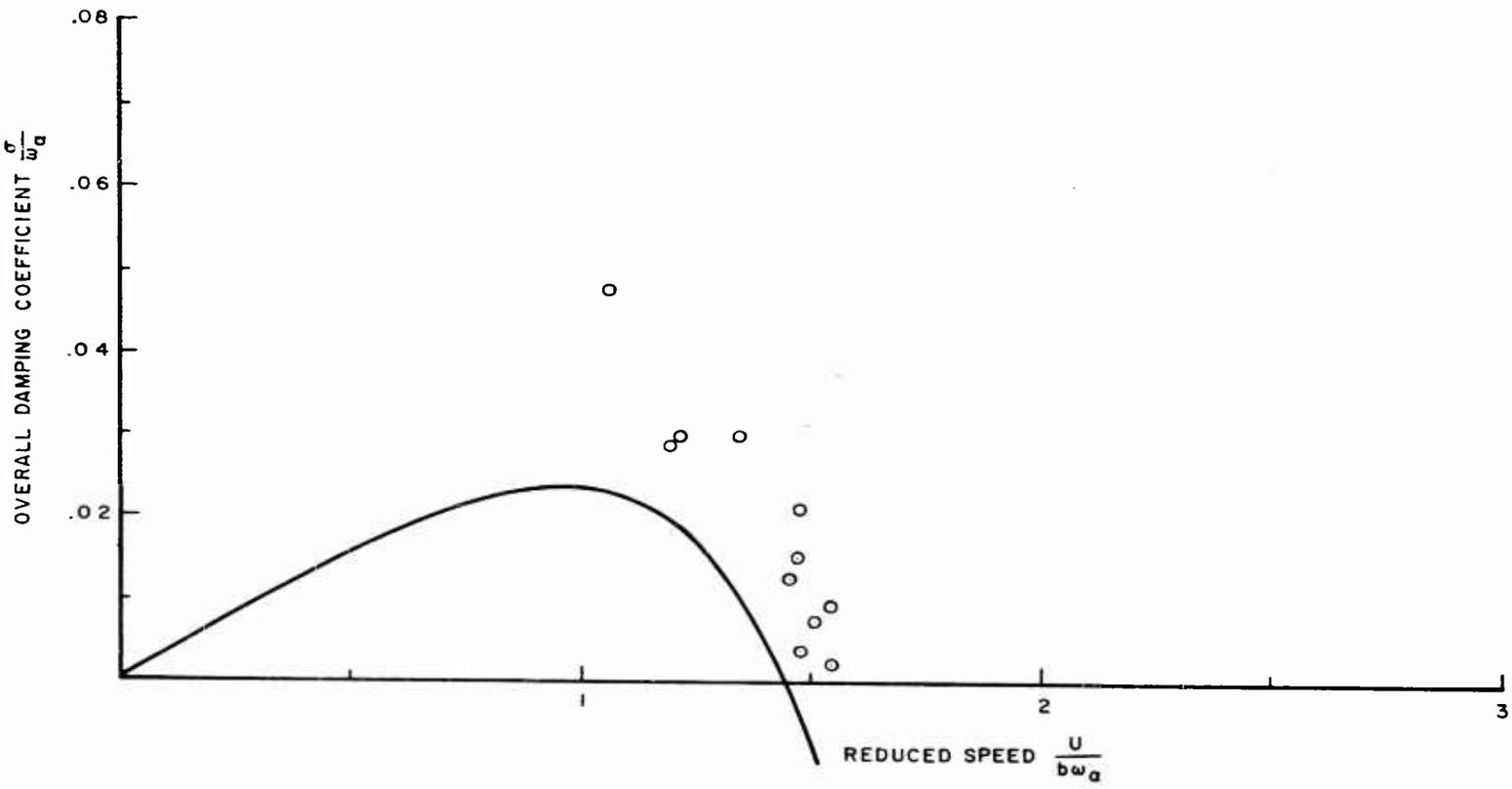

FIGURE 17. OVERALL DAMPING COEFFICIENT VERSUS REDUCED SPEED (STABILITY ANALYSIS, SERIES II, μ = 4.07)

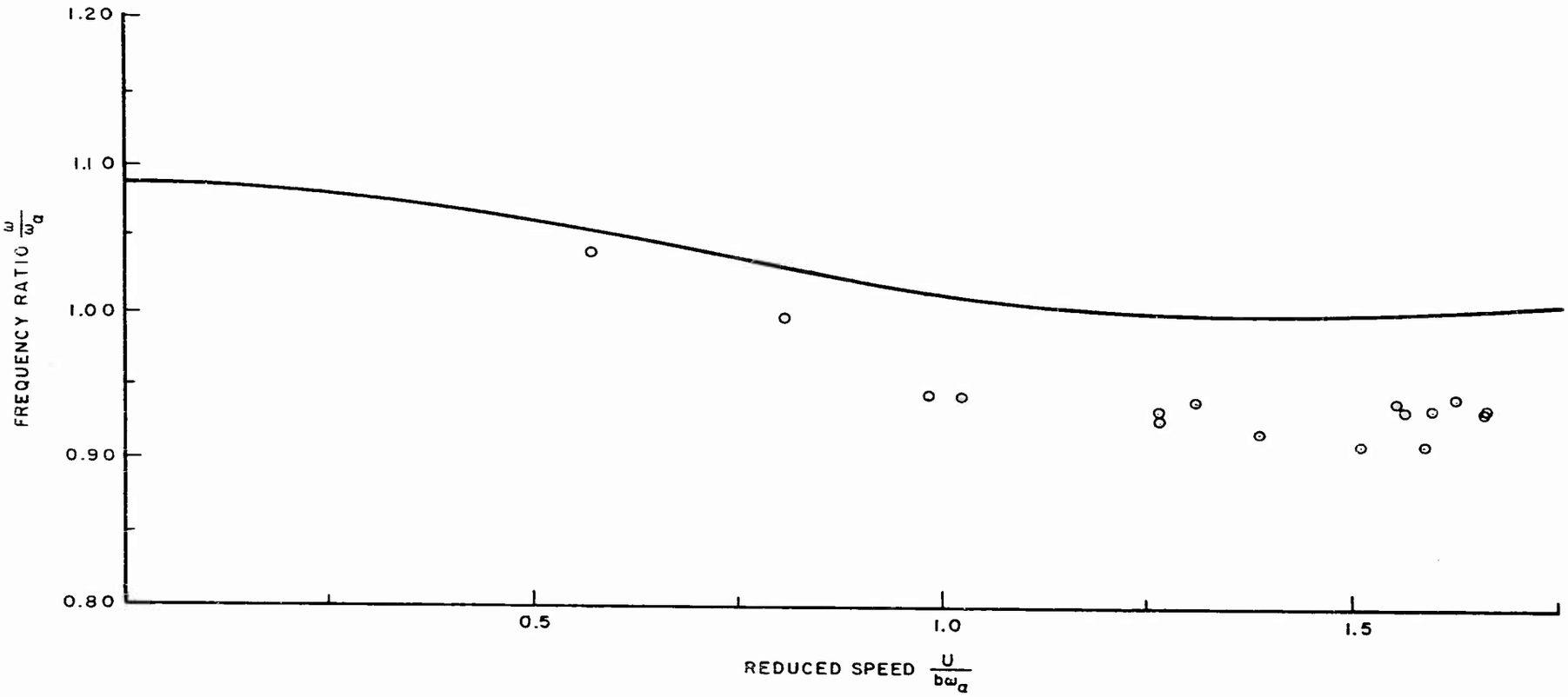

FIGURE 18. FREQUENCY RATIO VERSUS REDUCED SPEED (STABILITY ANALYSIS, SERIES 0, μ = 0.758)

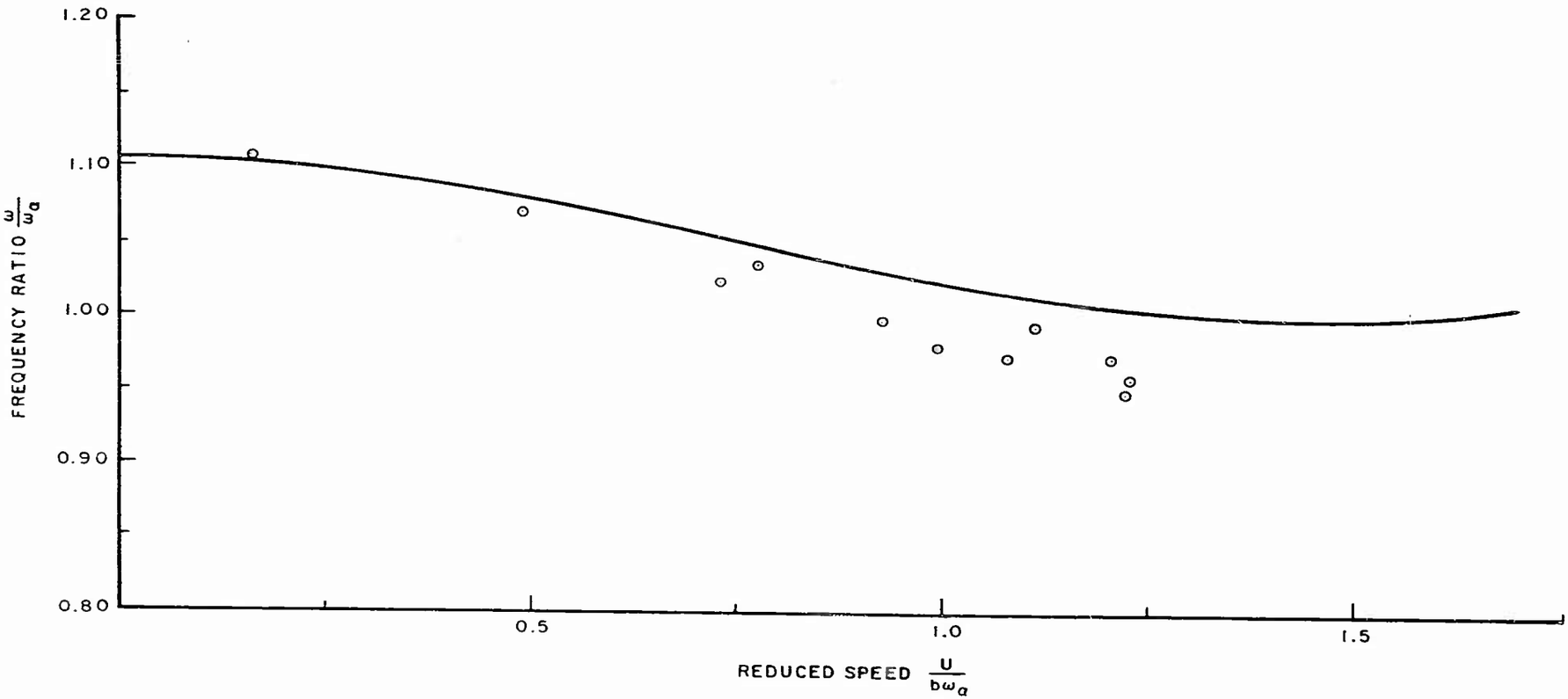

FIGURE 19. FREQUENCY RATIO VERSUS REDUCED SPEED (STABILITY ANALYSIS, SERIES 1, μ = 0.883)

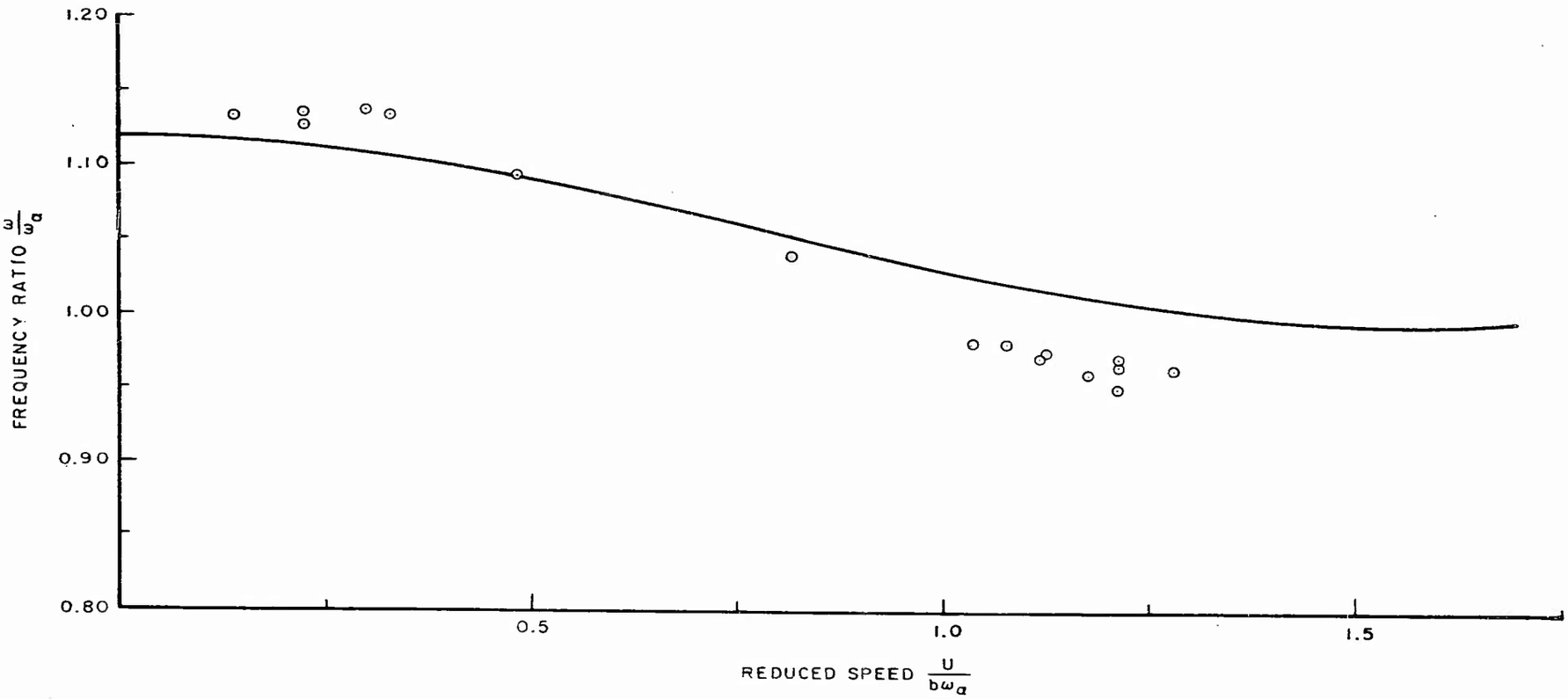

FIGURE 20. FREQUENCY RATIO VERSUS REDUCED SPEED (STABILITY ANALYSIS, SERIES 2, $\mu = 1.008$)

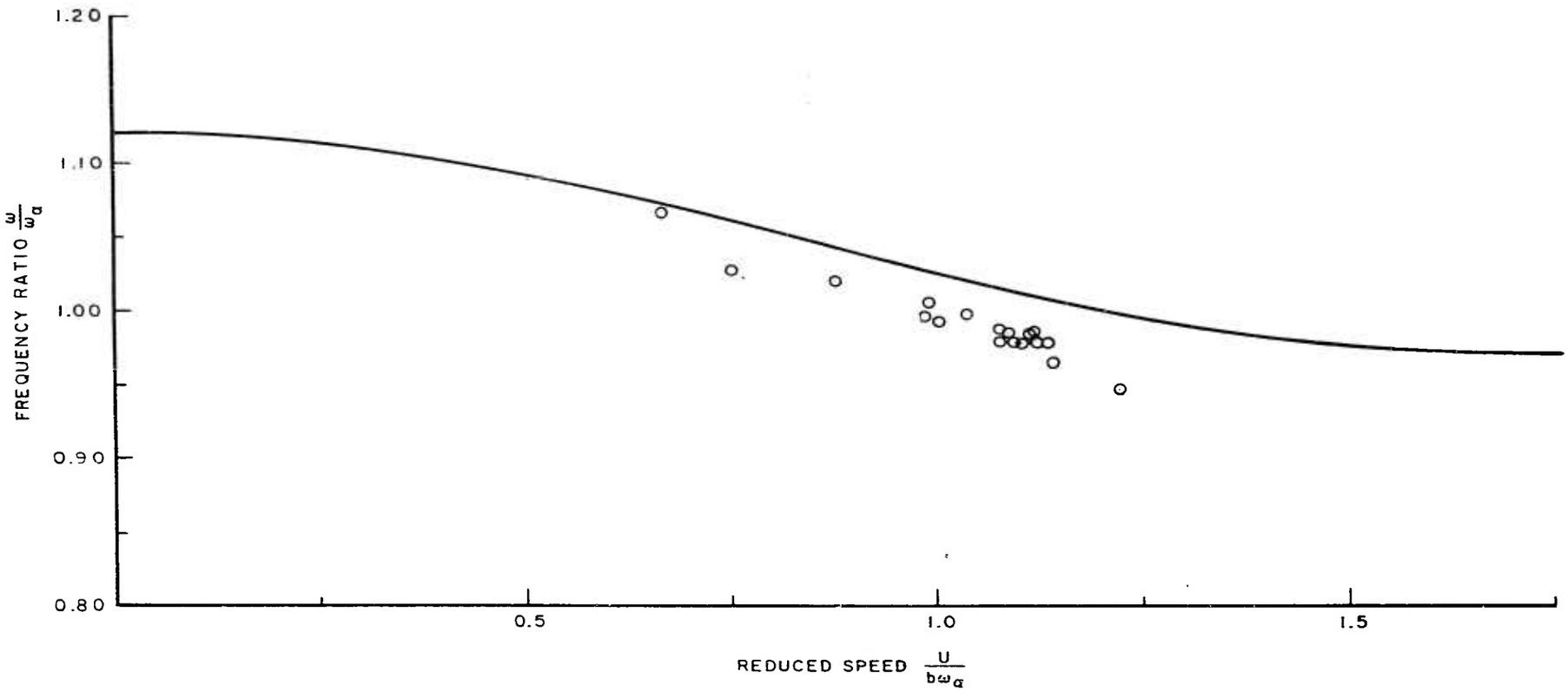

FIGURE 21. FREQUENCY RATIO VERSUS REDUCED SPEED (STABILITY ANALYSIS, SERIES 4, μ = 1.285)

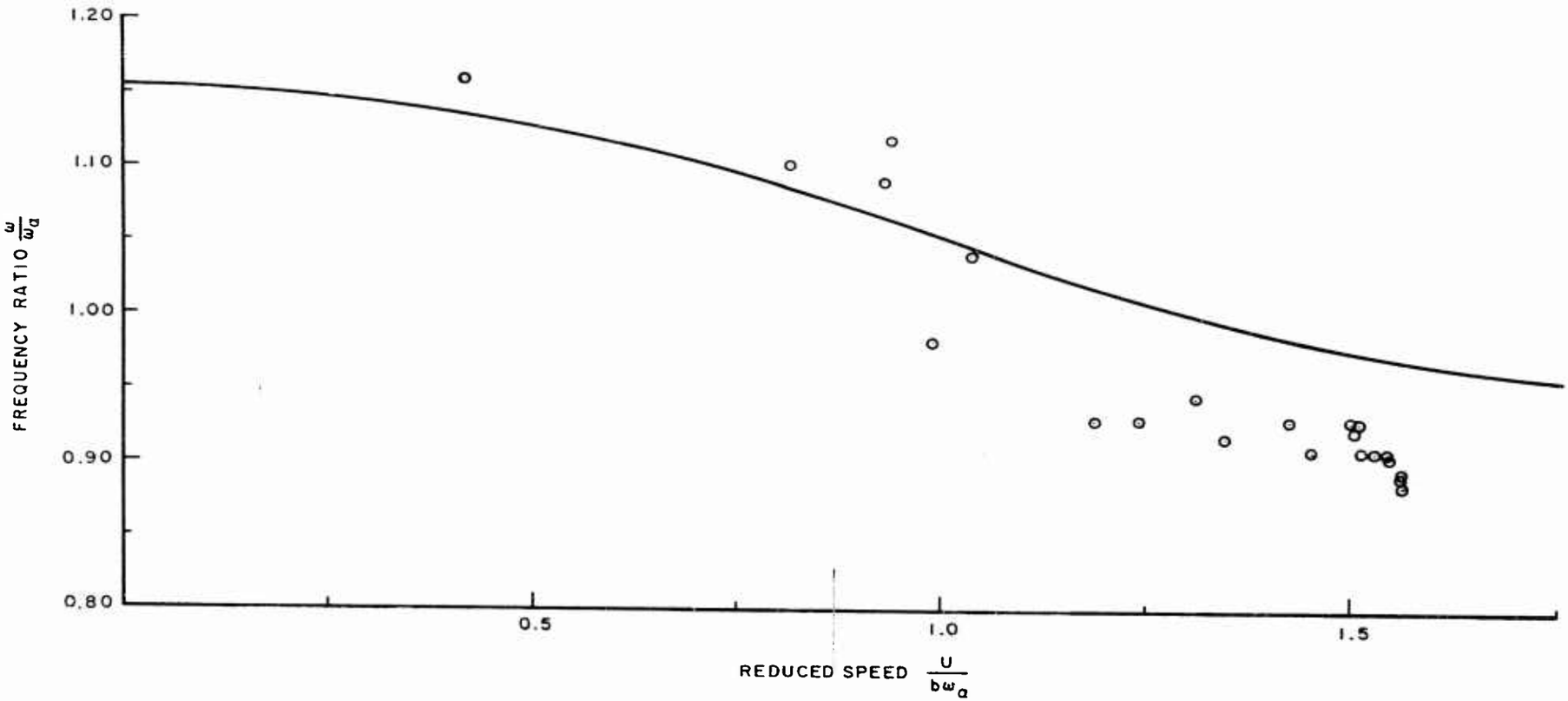

FIGURE 22. FREQUENCY RATIO VERSUS REDUCED SPEED (STABILITY ANALYSIS, SERIES 7, μ = 2.08)

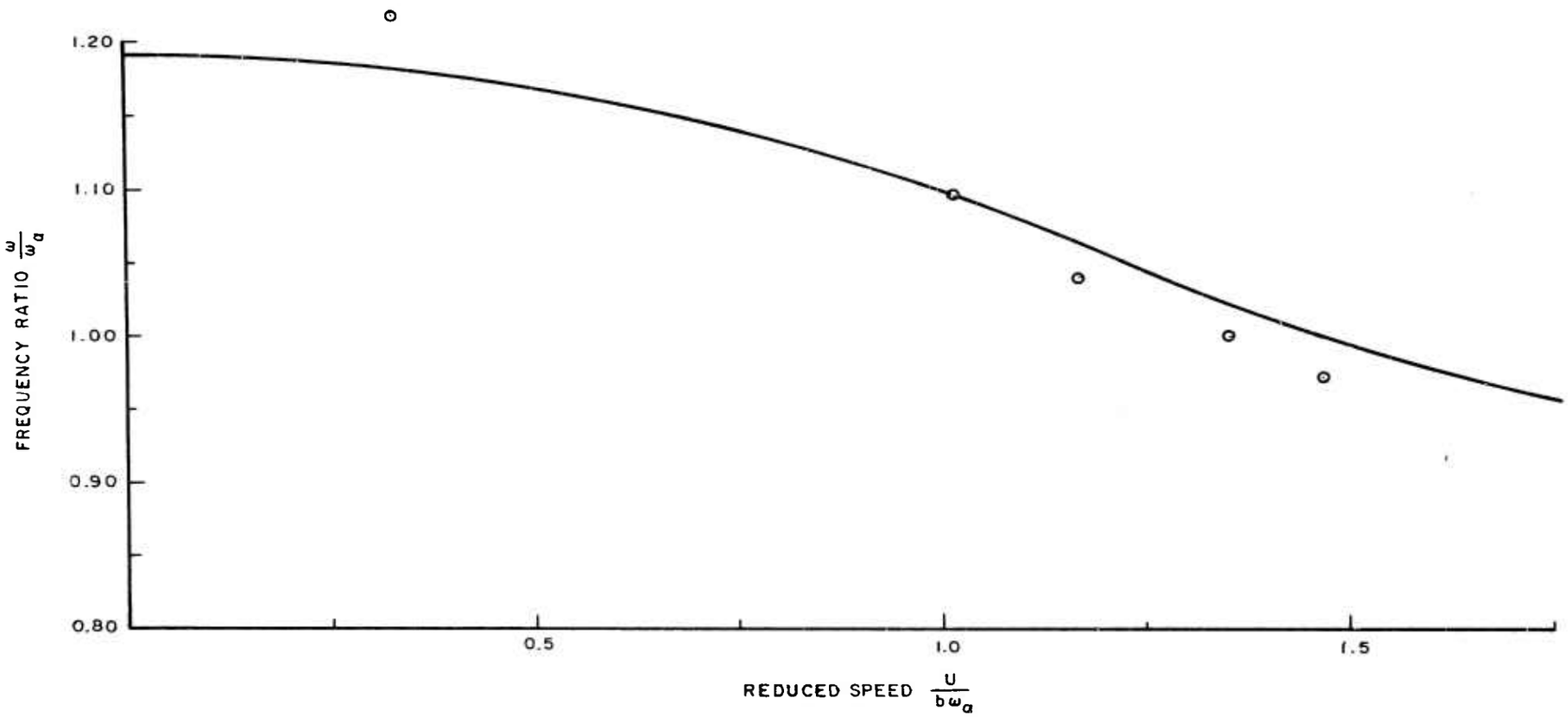

FIGURE 23. FREQUENCY RATIO VERSUS REDUCED SPEED (STABILITY ANALYSIS, SERIES 9, μ = 3.03)

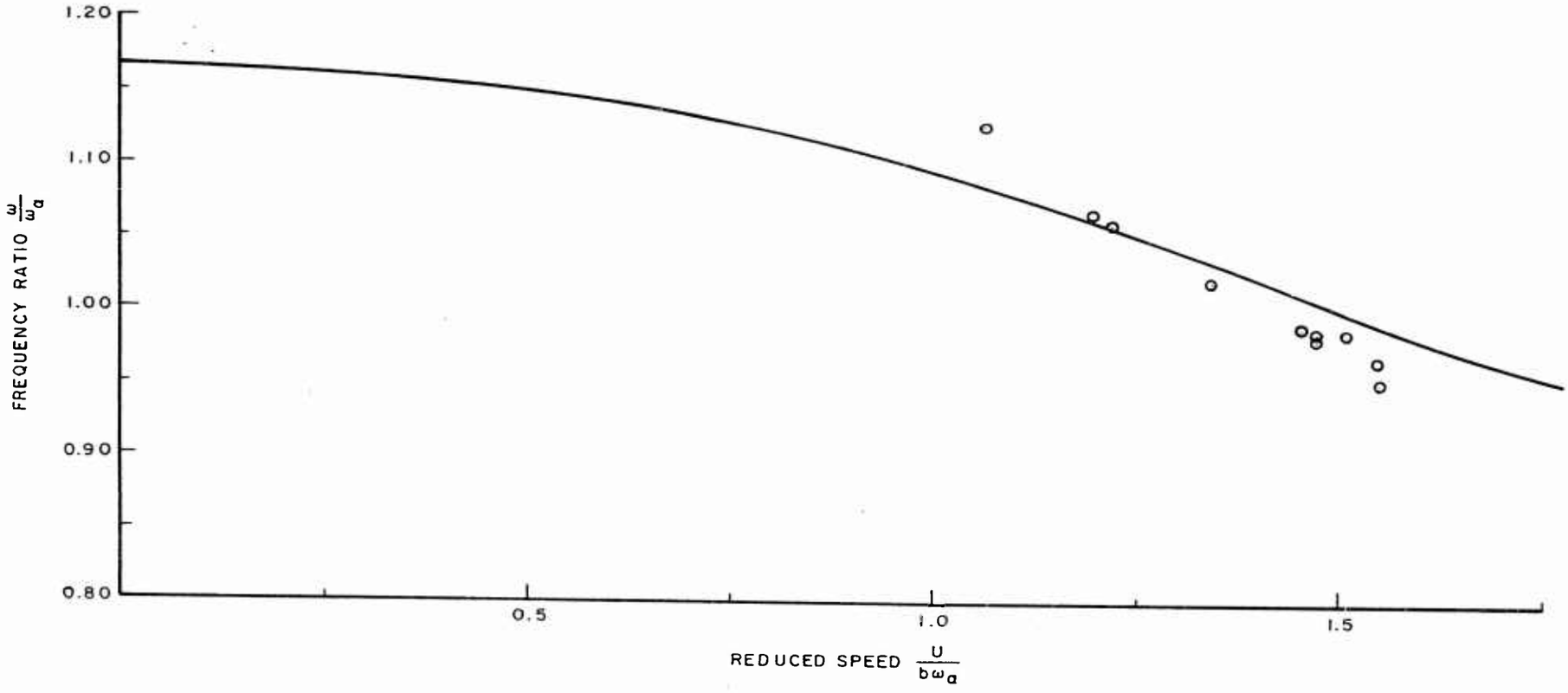

FIGURE 24. FREQUENCY RATIO VERSUS REDUCED SPEED (STABILITY ANALYSIS, SERIES II, μ = 4.07)

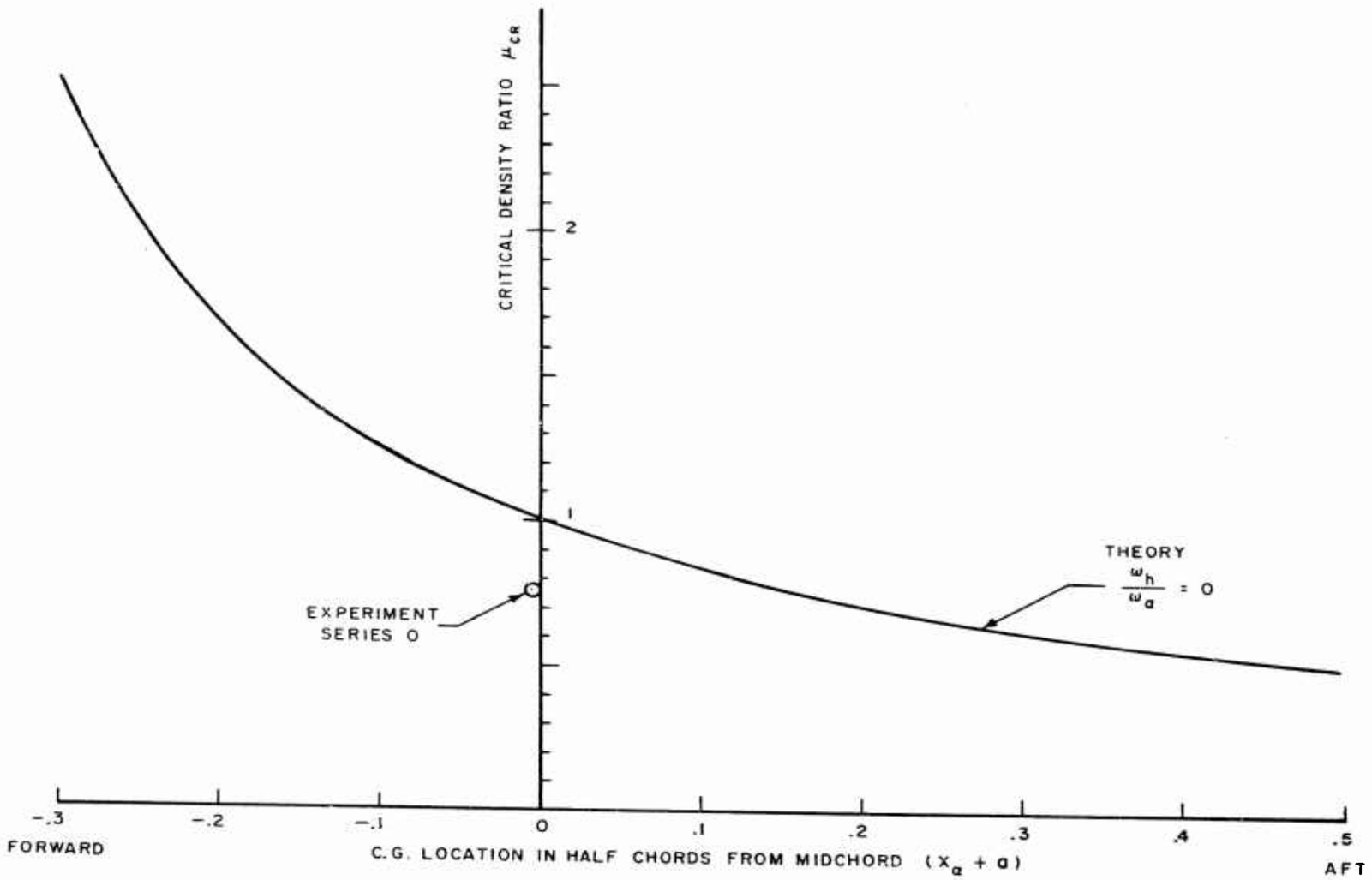

FIGURE 25. CRITICAL DENSITY-RATIO

APPENDIX A: STABILITY ANALYSIS BY SUPERPOSITION

I. INTRODUCTION

To predict the stability of small elastic-deformations of a hydrofoil section, three types of forces must be related to the motions of the foil: inertial reactions, elastic restraints, and hydrodynamic loads. The inertial forces can be described by either Lagrange's or Newton's equations; to describe the elastic forces, strain-displacement and stress-strain relationships must be established. (Hooke's law can be used to relate the stresses to the strains.) Hydrodynamic loads due to sinusoidal motions have been described mathematically by Theodorsen (reference 8).

A. HYDRODYNAMIC LOADS DUE TO SINUSOIDAL MOTIONS

The sinusoidal motions are expressed as

$$h(s) = h_o e^{jks}$$

$$\alpha(s) = \alpha_o e^{jks} \qquad \text{(A-1)}$$

where, h_o and α_o are small dimensionless amplitudes of heave and pitch, and may be complex; k is reduced frequency; and s is dimensionless time. The two-dimensional lift (L) and moment (M) per unit span for a sinusoidal motion are expressed as

$$L/\pi\rho bU^2 = -\left[h'' + \alpha' - a\alpha''\right] - 2C(k)\left[h' + \alpha + \left(\tfrac{1}{2} - a\right)\alpha'\right]$$

$$M/\pi\rho b^2U^2 = \left[ah'' - \left(\tfrac{1}{2} + a\right)\alpha' - \left(\tfrac{1}{8} + a^2\right)\alpha''\right] + 2\left(\tfrac{1}{2} + a\right)C(k)$$

$$\left[h' + \alpha + \left(\tfrac{1}{2} - a\right)\alpha'\right] \qquad \text{(A-2)}$$

$$\omega_n = \frac{2\pi}{T} n \; ; \; n = 1,2,3,\ldots \qquad \text{(A-5)}$$

Let $S = TU/b$ be the dimensionless period of the motion. Thus, the Fourier coefficients are

$$h_o = \frac{1}{S}\int_o^S h(s)\,ds, \qquad \alpha_o = \frac{1}{S}\int_o^S \alpha(s)\,ds,$$

$$h_n = \frac{2}{S}\int_o^S h(s)e^{-jk_n s}\,ds, \quad \alpha_n = \frac{2}{S}\int_o^S \alpha(s)e^{-jk_n s}\,ds. \qquad \text{(A-6)}$$

To find the lift response to this motion, the response for a single Fourier component must be obtained, which is expressed as

$$L_n/\pi\rho bU^2 = -e^{jk_n s}\left\{-k_n{}^2 h_n + \left[jk_n + ak_n^2\right]\alpha_n + 2C(k_n)\left[jk_n h_n + \left\{1 + \left(\frac{1}{2} - a\right)jk_n\right\}\alpha_n\right]\right\} \qquad \text{(A-7)}$$

and the moment response is expressed as

$$M_n/\pi\rho bU^2 = -e^{jk_n s}\left\{ak_n{}^2 h_n + \left[\left(\frac{1}{2} + a\right)jk_n - \left(\frac{1}{8} + a^2\right)k_n{}^2\right]\alpha_n - 2\left(\frac{1}{2} + a\right)C(k_n)\left[jk_n h_n + \left\{1 + \left(\frac{1}{2} - a\right)jk_n\right\}\alpha_n\right]\right\} \qquad \text{(A-8)}$$

The lift and moment response to h_o are zero; however, there is a steady response to the mean angle of attack (α_o):

$$L_o/\pi\rho bU^2 = -2\alpha_o = L_o'$$

$$M_o/\pi\rho b^2U^2 = +2\left(\frac{1}{2} + a\right)\alpha_o = M_o' \qquad \text{(A-9)}$$

The sum of the responses to the components of the motion (equation A-4) results in the total lift and moment:

and moment acting on the foil. Thus, the case of a foil operating in oblique seas may be analyzed. These results were derived assuming a rigid chord-section. Elastic deformations in camber could be included using the results of Spielberg*. The affects of aspect ratios as low as 2 can be included by using the table of aerodynamic coefficients by Reissner and Stevens**.

D. ARBITRARY MOTIONS

The Theodorsen results can be extended to arbitrary motions***. For this motion, the noncirculatory terms in equation A-10 are not changed and only terms containing $C(k_n)$ are considered. Also, the circulatory lift and moment terms depend on the motion in exactly the same way--that is, through the vertical velocity of the 3/4-chord point, which is

$$H'(s) = h'(s) + \alpha(s) + (\frac{1}{2} - a)\alpha'(s). \qquad (A\text{-}14)$$

Using this observation, the circulatory lift response to a single Fourier component of reduced frequency k is, for a unit amplitude of $H'(s)$,

$$\Delta L_c/\pi\rho U^2 b = - 2C(k)e^{jks} \qquad (A\text{-}15)$$

The Fourier integral representation of an arbitrary motion $H'(s)$ becomes

---

*Spielberg, Irvin, N., "The Two-Dimensional Incompressible Aerodynamic Coefficients for Oscillatory Changes in Airfoil Camber," Wright Air Development Center, Technical Note WCNS 52-7, 18 August 1952.

**Reissner, Eric and Stevens, John E., "Effect of Finite Span on the Airload Distributions for Oscillating Wings. II-Methods of Calculations and Examples of Application", NACA TN 1195, 1947.

***Wagner, H., "Uber die Entstehung des Dynamischen Auftriebes von Tragflugeln," Z. Ange. W. Math. Mech., Bd.5, Heft 1, February, 1925.

Consider, a step change in $H'(s)$:

$$H'(s) = \begin{cases} 0 , & \text{for } s < 0; \\ h'(0) + \alpha(0) + (\frac{1}{2} - a)\alpha'(0), & \text{for } s > 0 \end{cases} \qquad \text{(A-21)}$$

The Fourier integral for such a motion is

$$H'(s) = \frac{1}{2\pi}\left[h'(0) + \alpha(0) + (\frac{1}{2} - a)\alpha'(0)\right]\int_{-\infty}^{\infty} \frac{e^{jks}}{jk}\, dk \qquad \text{(A-22)}$$

Comparing equation A-22 and equation A-16 shows that

$$\eta(k) = \left[h'(0) + \alpha(0) + (\frac{1}{2} - a)\alpha'(0)\right]\frac{1}{jk} , \qquad \text{(A-23)}$$

for this motion. The circulatory lift response to this step change is found by substituting equation A-23 into equation A-18:

$$L_c/\rho U^2 b = -\left[h'(0) + \alpha(0) + (\frac{1}{2} - a)\alpha'(0)\right]\int_{-\infty}^{\infty} \frac{C(k)}{jk}\, e^{jks}\, dk \qquad \text{(A-24)}$$

The Wagner function $[\phi(s)]$ is defined as the time dependence of the circulator lift response to a unit step change in $H'(s)$ at $s = 0$ or

$$\phi(s) = \frac{1}{2\pi j}\int_{-\infty}^{\infty} \frac{C(k)}{jk}\, e^{jks}\, dk \qquad \text{(A-25)}$$

which when substituted into equation A-24 yields

$$L_c/\pi\rho U^2 b = -2\left[h'(0) + \alpha(0) + (\frac{1}{2} - a)\alpha'(0)\right]\phi(s) \qquad \text{(A-26)}$$

Dividing the Theodorsen function into its real and imaginary parts $[F(k)$ and $G(k)]$, respectively, results in two simpler relations for the Wagner function:

$$M = \pi\rho b^2U^2 \left[ah'' + \left(\frac{1}{2} + a\right)\alpha' + \left(\frac{1}{8} + a^2\right)\alpha'' \right] +$$

$$2\pi\rho b^2U^2 \left(\frac{1}{2} + a\right) \left\{ H'(0)\phi(s) + \int_0^s \phi(s - \gamma) \frac{d}{d\gamma} H'(\gamma)\, d\gamma \right\} \quad \text{(A-31)}$$

where

$$\phi(s) = \frac{2}{\pi}\int_0^\infty \frac{F(k)}{k} \sin ks \; dk , \quad \text{(A-32)}$$

$$H'(s) = \begin{cases} 0 & , s < 0; \\ h'(0) + U\alpha(0) + b\left(\frac{1}{2} - a\right)\alpha'(0) = H'(0), & s = 0; \\ h'(s) + U\alpha(s) + b\left(\frac{1}{2} - a\right)\alpha'(s) & , s > 0. \end{cases} \quad \text{(A-33)}$$

II. ANALYSIS OF SYSTEMS WITH TWO DEGREES-OF-FREEDOM

The lift and moment equations were used in the stability analysis to determine the overall damping and frequency ratio associated with the experimental conditions. To do this, equations A-30 through A-33 are substituted into the equations of motion, equations 18 and 19. The equations can be written as

$$(\mu + 1)h'' + \mu\Omega_h{}^2 h + (\mu\beta x_\alpha - a)\alpha'' + \alpha' + 2\left[H'(0)\phi(s) + \int_0^s \phi(s - \gamma)H''(\gamma)\, d\gamma\right] = 0 \quad \text{(A-34)}$$

and

$$(\mu\beta x_\alpha - a)h'' + (\mu r_\alpha^2 + \frac{1}{8} + a^2)\alpha'' + \left(\frac{1}{2} - a\right)\alpha' + \mu r_\alpha^2 \Omega_\alpha^2 \alpha + 2\left[H'(0)\phi(s) + \int_0^s \phi(s - \gamma)H''(\gamma)\, d\gamma\right] = 0. \quad \text{(A-35)}$$

$$Q_h = \mu r_\alpha^2 \Omega_\alpha^2 - (\tfrac{1}{4} - a^2)\mu\Omega_h^2$$

$$Q_i = -(\tfrac{1}{2} + a)\mu\Omega_h^2 \qquad \text{(A-36 cont'd)}$$

$$P_a = h_o Q_a$$

$$P_b = h_o Q_b$$

$$P_c = h_o(\mu + 1)\mu r_\alpha^2 \Omega_\alpha^2 + \alpha_o(\mu\beta x_\alpha - a)\mu r_\alpha^2 \Omega_\alpha^2$$

$$P_d = \alpha_o \mu r_\alpha^2 \Omega_\alpha^2$$

$$P_e = 0$$

$$P_f = h_o Q_f$$

$$P_g = h_o[1 - (\mu + 1)(\tfrac{1}{2} + a) - (\mu\beta x_\alpha - a)] - \alpha_o[(\tfrac{1}{2} + a)(\mu\beta x_\alpha - a) + \mu r_\alpha^2 + \tfrac{1}{8} + a^2]$$

$$P_h = h_o \mu r_\alpha^2 \Omega_\alpha^2 + \alpha_o[(\tfrac{1}{2} - a)\mu r_\alpha^2 \Omega_\alpha^2 - 1]$$

$$P_i = 0 \qquad \text{(A-37)}$$

$$R_a = \alpha_o Q_a$$

$$R_b = \alpha_o Q_b$$

$$R_c = \alpha_o(\mu r_\alpha^2 + \tfrac{1}{8} + a^2)\mu\Omega_h^2 + h_o(\mu x_\alpha - a)\mu\Omega_h^2$$

$$R_d = \alpha_o Q_d$$

$$R_e = 0$$

$$R_f = \alpha_o Q_f$$

$$R_g = \alpha_o$$

$$R_h = [h_o + (\tfrac{1}{2} - a)\alpha_o] Q_i$$

$$R_i = 0 \qquad \text{(A-38)}$$

The polynomials in equation 44 are now defined so that the inverse Laplace transform is introduced to determine $h(s)$ and $\alpha(s)$. Referring to any text on Laplace transformation the following theorem applies*. If $Q(p)$ is a polynomial of degree i, with i distinct zeros $p = p_1, p_2, \ldots, p_i$, and $P(p)$ is a polynomial of degree i - 1 or less, then

$$\frac{P(p)}{Q(p)} = \sum_{n=1}^{i} \frac{P(p_n)}{Q'(p_n)} \cdot \frac{1}{(p - p_n)} \qquad \text{(A-43)}$$

To each term of equation A-43 the following inverse transform applies

$$\mathcal{L}^{-1}\left\{\frac{1}{p - p_n}\right\} = e^{p_n t} \qquad \text{(A-44)}$$

Summing this result for each of the six zeros of $Q(p)$ yields

$$\mathcal{L}^{-1}\left\{\frac{P(p)}{Q(p)}\right\} = \sum_{n=1}^{6} \frac{P(p_n)}{Q'(p_n)} e^{p_n s} \qquad \text{(A-45)}$$

The six roots of the denominator $[Q(p)]$ must be determined. A process based on Newton's iterative method was used.** In this process, the quadratic factors of equation 46 are determined first, then the pairs of roots for each quadratic factor are found. The polynomial to be factored is of sixth order so that three quadratic factors and six roots must be determined.

Each root is complex:

$$p_n = u_n + jv_n$$

$$n = 1, \ldots, 6 \qquad \text{(A-46)}$$

---

*Hildebrand, F. B., ADVANCED CALCULUS FOR ENGINEERS, Prentice-Hall, Inc., New York, 1954.

**Described in Scarborough, J. B., NUMERICAL MATHEMATICAL ANALYSIS, The Johns Hopkins Press, Baltimore, 1950.

APPENDIX B: GENERALIZATION OF THEODORSEN'S FUNCTION FOR CONVERGENT (STABLE) OSCILLATIONS

by Paul Ritger

The Theodorsen function (reference B-1) was developed for the case of a real argument. When this function was extended to include complex arguments, two different and incompatible conclusions were made. (references B-2 and B-3) To resolve this discrepancy, the following rigorous analysis was developed.

Theodorsen (reference B-1) showed that the circulational part of lift forces caused by translational motions with unit-magnitude velocities--that is, $h(s) = e^{j\zeta s}$--is

$$L(s) = 2\rho\pi Ubc(\zeta)h'(s) \tag{B-1}$$

where the Theodorsen function $C(\zeta)$ is

$$C(\zeta) = \frac{\displaystyle\int_1^\infty \frac{x}{\sqrt{x^2 - 1}}\, e^{-j\zeta x}\, dx}{\displaystyle\int_1^\infty \sqrt{\frac{x+1}{x-1}}\, e^{-j\zeta x}\, dx} \tag{B-2}$$

The function $C(\zeta)$ is properly defined by equation B-2, if and only if the complex number ζ is restricted so that

$$\mathrm{Im}(\zeta) < 0 \tag{B-3}$$

This inequality is satisfied in the case of divergent oscillations. If $\mathrm{Im}(\zeta) = 0$, the integrands in equation B-2 behave like $\sin \zeta x$ at ∞; hence, the integrals would be oscillatory divergent. If $\mathrm{Im}(\zeta) > 0$, which is true for convergent oscillations, then both integrals in equation B-2 become infinite. Hence, the Theodorsen function, as defined by equation B-2, is meaningless for $\mathrm{Im}(\zeta) \geq 0$.

points then it is essential to specify which branch of the function is to be used. In the present case,the physically correct branch is partly determined by equation B-2. That is, we must be sure to choose a branch of $C_1(\zeta)$ that coincides with $C(\zeta)$ for $\mathrm{Im}(\zeta) < 0$, i.e., $-\pi < \arg\ \zeta < 0$. If the so-called "principal branch" of $K_n(j\zeta)$ is chosen, this condition is satisfied and, hence, this seems to be the most natural choice. Luke and Dengler have used another branch as will be shown below.

The "principal branch" of $K_n(j\zeta)$ is usually defined (see Watson, reference B-5, p. 77) in terms of the function I_n. That is, in general, we have the following definition of the many-valued function $K_n(z)$

$$K_n(z) = \frac{\pi}{2} \lim_{\nu \to n} \frac{I_{-\nu}(z) - I_\nu(z)}{\sin \nu\pi}, \qquad (z \neq 0). \qquad \text{(B-6)}$$

Now, $I_\nu(z)$ is in turn defined in terms of $J_\nu(z)$ and the principal branch of $I_\nu(z)$ is given by

$$I_\nu(z) = \begin{cases} e^{-\nu\pi j/2}\ J_\nu(ze^{\pi j/2}), & -\pi < \arg\ z \leq \pi/2, \\ e^{3\nu\pi j/2}\ J_\nu(ze^{-3\pi j/2}), & \pi/2 < \arg\ z \leq \pi. \end{cases} \qquad \text{(B-7)}$$

In equation B-7, to be precise, the principal branch of J_ν is to be taken, which is the reason for a split definition of $I_\nu(z)$. If z in equation B-7, lies in the second quadrant, i.e., $\pi/2 < \arg\ z \leq \pi$, then $ze^{\pi j/2}$ (i.e. jz) would be such that $\pi < \arg\ (ze^{\pi j/2}) \leq 3\pi/2$ but this would then give a value of J_ν which is not on the principal branch. The principal branch of $J_\nu(\zeta)$ (see Watson p. 44) is obtained by restricting $\arg\ \zeta$ to $-\pi < \arg\ \zeta \leq \pi$.

To carry this all the way, J_ν is defined by

$$J_\nu(\zeta) = (\zeta^\nu) \sum_{K=0}^{\infty} a_K(\zeta^K)$$

This definition of $K_n(z)$ is often written

$$K_n(z) = \frac{\pi}{2} j e^{n\pi j/2} H_n^{(1)}(jz) \qquad \text{(B-12)}$$

which is correct for the multi-valued function $K_n(z)$, but if one wishes to restrict oneself to the principal branch, then equation B-11 must be used.

The results of Luke and Dengler are obtained by using equation B-12 instead of equation B-11 and hence must be interpreted with this fact in mind. In particular, they are concerned with the values of $C(\zeta)$ in the vicinity of arg $\zeta = 0$. Hence, by equation B-5 they use $K_n(j\zeta)$ near where arg $\zeta = 0$, i.e. where arg $j\zeta = \pi/2$. So, if arg ζ is slightly greater than zero, they are using values which are no longer on the principal branch. The many valued function $K_n(j\zeta)$ is continuous for arg $\zeta = 0$, but the single-valued principal branch is not. Jones used the principal branch and hence his values show this discontinuity along arg $\zeta = 0$. Incidentally, he uses rectangular coordinates which hide the significance of the restriction on arg ζ.

Since aerodynamicists seem to be most interested in the region around arg $\zeta = 0$, there is something to be said for the Luke and Dengler approach. That is, their extension of the definition of $C(k)$ is the only one which agrees with equation B-1 for $\mathrm{Im}(k) < 0$ and at the same time is the analytic continuation of equation B-1 across the half-line arg $k = 0$. It should be emphasized, however, that this approach still leaves one with a discontinuity along the negative real axis, i.e. for arg $\zeta = \pm \pi$ (if one desires a single-valued function). Since Luke and Dengler do not discuss the branches of functions involved, there is some ambiguity in their definitions.

Moreover, the physical meaning of equation B-5 for $\mathrm{Im}(\zeta) \geq 0$ is not at all clear.

Hence, the circulational part of the lift force caused by a unit step change in translational velocity is given in general by

$$L(s) = 2\rho\pi Ub \left[\phi(s) + j\zeta \int_0^s \phi(x)\, e^{j\zeta(s-x)}\, dx\right] \quad \text{(B-16)}$$

This result agrees with Bisplinghoff, etc. (reference B-7) for a lift force.

REFERENCES

B-1. Theodorsen, Th.: "General Theory of Aerodynamic Instability and the Mechanism of Flutter," NACA T.T. No. 496, 1935.

B-2. Jones, W. P.: "Aerodynamic Forces on Wings in Non-Uniform Motion," R. and M. No. 2117, August 1945.

B-3. Luke, Y. L. and Dengler, M. A.: "Tables of the Theodorsen Circulation Function for Generalized Motion," Journal Aero. Sciences, Vol. 18, No. 7, pp. 478-483, July 1951.

B-4. Sears, W. R.: "Some Aspects of Non-Stationary Airfoil Theory and its Practical Application," Jour. Aero. Sciences, Vol. 8, No. 3, p. 104.

B-5. Watson, G. N.: "A Treatise on the Theory of Bessel Functions," Second Edition, Cambridge University Press, 1952.

B-6. Van de Vooren, A. I.: "Generalization of the Theodorsen Function to Stable Oscillations," Jour. Aero. Sciences, Vol. 19, No. 3, Readers Forum, pp. 209-211, March 1952.

B-7. Bisplinghoff, Ashley, Halfman: "Aeroelasticity," Chapter 5, Addison-Wesley, 1957.

DISTRIBUTION LIST

Copies

7 Chief
Bureau of Ships
Department of the Navy
Washington 25, D.C.
Attn: Information Branch (Code 335) (3)
Preliminary Design (Code 420) (1)
Hull Design (Code 440) (3)

50 Commanding Officer and Director
David Taylor Model Basin
Washington 7, D.C.
Attn: (Code 513)

2 St. Anthony Falls Hydraulic Laboratory
University of Minnesota
Minneapolis, Minnesota
Attn: Prof. B. Silberman
Mr. J. N. Wetzel

2 Chief of Naval Research
Fluid Dynamics Branch
Department of the Navy
Washington 25, D.C.
Attn: (Code 438)

1 Chief
Bureau of Naval Weapons
Dynamics Sub Unit
Washington 25, D.C.
Attn: Mr. D. Michel
(Code RAAD-222)

1 Commander
U.S. Naval Ordnance Laboratory
White Oak, Maryland

1 Commander
U.S. Naval Ordnance Test Station
China Lake, California

2 Officer-in-charge, Pasadena Annex
U.S. Naval Ordnance Test Station
Oceanic Research (Code P-508)
3202 E. Foothill Blvd.
Pasadena 8, California

2 Director
National Bureau of Standards
Washington 25, D.C.
Attn: Dr. G. B. Schubauer, Chief
Fluid Mechanics Section
Dr. J. M. Franklin, Consultant

2 Director
Langley Research Center
Langley Field, Virginia
Attn: Mr. I. E. Garrick
Mr. D. J. Marten

1 National Research Council of Canada
Hydromechanics Laboratory
Ottawa 2, Canada

Copies

1 Office of Research and Development
Maritime Administration
441 G. Street, N.W.
Washington 25, D.C.
Attn: Mr. R. P. Godwin, Acting Chief

10 Commander
Armed Services Technical Info. Agency
Arlington Hall Station
Arlington 12, Virginia
Attn: TIPDR

1 Commander
Air Research and Development Command
Air Force Office of Scientific Research
14th and Constitution
Washington 25, D.C.
Attn: Mechanics Branch

1 Commander
Wright Air Development Division
Aircraft Laboratory
Wright-Patterson Air Force Base, Ohio
Attn: Mr. W. Mykytow, Dynamics Branch

1 Boeing Airplane Co.
Seattle Division
Seattle, Washington
Attn: Mr. M. J. Turner

3 California Institute of Technology
Pasadena, California
Attn: Dr. M.S. Plesset
Dr. T. Y. Wu
Dr. A. J. Acosta

2 Convair
P.O. Box 1950
San Diego 12, California
Attn: Mr. A. D. MacLellan
Systems Dynamics Group
Mr. H. T. Brooke
Hydrodynamics Group

2 Cornell Aeronautical Laboratory
4455 Genesee Street
Buffalo, New York
Attn: Mr. W. Targoff
Mr. R. White

3 Electric Boat Division
General Dynamics Corp.
Groton, Conn.
Attn: Mr. Robert McCandliss

1 General Applied Sciences Laboratories, Inc.
Merrick and Stewart Avenues
Westbury, Long Island, New York
Attn: Dr. F. Lane

1 Gibbs and Cox, Inc.
21 West Street
New York, New York

Copies

1 Grumman Aircraft Engineering Corp.
Dynamic Developments Division
Babylon, New York

2 Grumman Aircraft Engineering Corp.
Bethpage, Long Island, New York
Attn: Mr. E. Baird
Mr. E. Bower

2 President
Hydronautics, Inc.
200 Monroe Street
Rockville, Maryland

1 Lockheed Aircraft Corp.
Missiles and Space Division
Palo Alto, California
Attn: R. W. Kermeen

3 Massachusetts Institute of Technology
Fluid Dynamics Research Laboratory
Cambridge 39, Massachusetts
Attn: Prof. H. Ashley
Prof. M. Landahl
Prof. J. Dugundji

1 Midwest Research Institute
425 Volker Blvd.
Kansas City 10, Missouri
Attn: Mr. Zeydel

1 Ordnance Research Laboratory
Pennsylvania State University
University Park, Pennsylvania
Attn: Dr. M. Sevik

3 Director
Department of Mechanical Sciences
Southwest Research Institute
8500 Culebra Road
San Antonia 6, Texas
Attn: Dr. H. N. Abramson
Mr. G. Ransleben
Editor, Applied Mechanics Review

Copies

2 Stanford University
Department of Mathematics
Stanford, California
Attn: Dr. B. Perry
Dr. E. Y. Hsu

1 State University of Iowa
Iowa Institute of Hydraulic Research
Iowa City, Iowa
Attn: Prof. L. Landweber

2 Technical Research Group, Inc.
2 Aerial Way
Syosset, Long Island, New York
Attn: Dr. Jack Kotik

1 The Rand Corp.
1700 Main Street
Santa Monica, California
Attn: Dr. B. Parkin

1 University of California
Department of Engineering
Institute of Engineering Research
Berkeley, California
Attn: Dr. J. V. Wehausen

1 Department of Naval Architecture
University of California
Berkeley, California
Attn: Prof. H. A. Schade, Head

ADDITIONS TO DISTRIBUTION LIST

Copies

1 Commanding Officer
Office of Naval Research
Branch Office
The John Crerar Library Bldg.
86 East Randolph Street
Chicago 1, Illinois

1 Commanding Officer
Office of Naval Research
207 West 24th Street
New York 11, New York

1 Commanding Officer
Office of Naval Research
Branch Office
1030 East Green Street
Pasadena 1, California

1 Commanding Officer
Office of Naval Research
Branch Office
495 Summer Street
Boston 10, Massachusetts

1 Commanding Officer
Office of Naval Research
Branch Office
1000 Geary Street
San Francisco 9, California

10 Commanding Officer
Office of Naval Research
Branch Office
Navy #100, Box 39
Fleet Post Office
New York, New York

2 Director
U.S. Naval Research Laboratory
Washington 25, D.C.

1 Oceanics
114 East 40th Street
New York 16, New York

Davidson Laboratory Report No. 856 UNCLASSIFIED

HYDROFOIL FLUTTER PHENOMENON AND AIRFOIL FLUTTER THEORY, VOLUME I, by Charles J. Henry, September 1961

The theoretical procedures commonly used by aerolasticians were applied to predict the flutter speed of a rigid hydrofoil that had two degrees of freedom. The results, compared with corresponding experimental measurements, indicated a discrepancy between theoretical and experimental flutter speed at low-density ratios; the predicted asymptotic behavior of flutter speeds occurred, but at a lower density ratio. In addition, the accuracy of the circulation terms is more doubtful than that of the added mass and linear terms in the theory.

Davidson Laboratory Report No. 856 UNCLASSIFIED

HYDROFOIL FLUTTER PHENOMENON AND AIRFOIL FLUTTER THEORY, VOLUME I, by Charles J. Henry, September 1961

The theoretical procedures commonly used by aerolasticians were applied to predict the flutter speed of a rigid hydrofoil that had two degrees of freedom. The results, compared with corresponding experimental measurements, indicated a discrepancy between theoretical and experimental flutter speed at low-density ratios; the predicted asymptotic behavior of flutter speeds occurred, but at a lower density ratio. In additon, the accuracy of the circulation terms is more doubtful than that of the added mass and linear terms in the theory.

Davidson Laboratory Report No. 856 UNCLASSIFIED

HYDROFOIL FLUTTER PHENOMENON AND AIRFOIL FLUTTER THEORY, VOLUME I, by Charles J. Henry, September 1961

The theoretical procedures commonly used by aerolasticians were applied to predict the flutter speed of a rigid hydrofoil that had two degrees of freedom. The results, compared with corresponding experimental measurements, indicated a discrepancy between theoretical and experimantal flutter speed at low-density ratios; the predicted asymptotic behavior of flutter speeds occurred, but at a lower density ratio. In addition, the accuracy of the circulation terms is more doubtful than that of the added mass and linear terms in the theory.

Davidson Laboratory Report No. 856 UNCLASSIFIED

HYDROFOIL FLUTTER PHENOMENON AND AIRFOIL FLUTTE THEORY, VOLUME I, by Charles J. Henry, September 1961

The theoretical procedures commonly used by aerolasticians were applied to predict the flutter speed of a rigid hydrofoil that had two degrees of freedom. The results, compared with corresponding experimental measurements, indicated a discrepancy between theoretical and experimental flutter speed at low-density ratios; the predicted asymptotic behavior of flutter speeds occurred, but at a lower density ratio. In addition, the accuracy of the circulation terms is more doubtful tha that of the added mass and linear terms in the theory.